**Universidade Federal do Rio Grande do Norte**
**Centro de Ciências Exatas e da Terra**
**Programa de Pós-Graduação em Geodinâmica e Geofísica**

**DISSERTAÇÃO DE MESTRADO**

# EVIDÊNCIAS GEOFÍSICAS DE DOMEAMENTO NA ESTRUTURAÇÃO PROFUNDA DA PORÇÃO CENTRAL DA FAIXA SERIDÓ (NE - BRASIL)

Autora:

**Nitzschia Regina Rodrigues Domingos**

Orientador:

**Prof. Dr. Walter Eugênio de Medeiros (PPGG/UFRN)**

Coorientador:

**Dr. Roberto Gusmão de Oliveira (CPRM/SGB)**

**Dissertação nº 241/PPGG**

**Natal-RN**

**Janeiro de 2020**

**Universidade Federal do Rio Grande do Norte**
**Centro de Ciências Exatas e da Terra**
**Programa de Pós-Graduação em Geodinâmica e Geofísica**

**DISSERTAÇÃO DE MESTRADO**

# EVIDÊNCIAS GEOFÍSICAS DE DOMEAMENTO NA ESTRUTURAÇÃO PROFUNDA DA PORÇÃO CENTRAL DA FAIXA SERIDÓ (NE - BRASIL)

Autora:

**Nitzschia Regina Rodrigues Domingos**

Dissertação apresentada em 08 de janeiro de dois mil e vinte, ao Programa de Pós-Graduação em Geodinâmica e Geofísica - PPGG, da Universidade Federal do Rio Grande do Norte - UFRN como requisito à obtenção do Título de Mestre em Geodinâmica e Geofísica, com área de concentração em Geofísica.

Comissão Examinadora:

**Prof. Dr. Walter Eugênio de Medeiros (PPGG/UFRN) - Orientador**

**Prof. Dr. Carlos José Archanjo (IGc/USP) - Examinador externo**

**Dr. Vladimir Cruz de Medeiros (CPRM/SGB) - Examinador externo**

**Natal-RN**

**Janeiro de 2020**

***Ao meu avô Geraldo (em memória).***

# Agradecimentos

Ao meu orientador Professor Dr. Walter Eugênio de Medeiros pela orientação, discussões e incentivo contínuo durante estes anos. Agradeço por contribuir com o meu desenvolvimento como pesquisadora e pela confiança em mim depositada.

Ao meu coorientador e colega de trabalho Roberto Gusmão de Oliveira, exemplo de ética, caráter, competência e profissionalismo. Meus sinceros agradecimentos por todo o esforço empregado para a realização deste Mestrado. Obrigada pelo tempo e presteza dedicados à coorientação e esclarecimentos geológicos e geofísicos indispensáveis a este trabalho.

Ao Serviço Geológico do Brasil pela minha liberação para o Mestrado e pela cessão dos dados aerogeofísicos, gravimétricos terrestres e de densidade e susceptibilidade magnética dos testemunhos de sondagem do furo FD-SE-001 – Riacho Fechado, necessários ao estudo. Agradeço aos meus colegas diretores, gerentes e supervisores (passados e presentes), em especial à Ana Cláudia Accioly, Fátima Lyra, Silvana Melo, Luiz Gustavo, Geysson e Felipe Lima. Ainda agradeço aos meus amigos e colegas de trabalho, Roberta Galba, Silvana Diene, Cleide Moura, André Cunha, Izaac Cabral, Priscila Rezende, Caio Pereira, Frank Gurgel, Fernanda Barbosa, Alexandre Ranier, Edlene, Angélica Lima e Janaína pelas discussões e incentivo.

Ao Programa de Pós-Graduação em Geodinâmica e Geofísica (PPGG/UFRN) e ao seu atual coordenador Prof. Dr. Moab Praxedes Gomes pela assistência. Aos professores membros do Programa pelos ensinamentos e trocas de ideias. Ao secretário Thalles Pinto pela disponibilidade em ajudar e informar. Aos colegas de pós-graduação Juliana, Renata, Gilberto, Augusto, Ricardo e Alexandre pela troca de conhecimento e bons momentos de convivência. Agradeço ainda à querida Elizângela, colega de pós-

graduação por alguns meses e que se tornou uma amiga. Obrigada pelo encorajamento constante, conhecimentos compartilhados e pelos bons momentos usufruídos.

Gostaria de agradecer ao colega Dr. Vladimir Cruz de Medeiros, ao Prof. Dr. Francisco Hilário Rego Bezerra e ao Prof. Dr. Carlos José Archanjo pela participação como membros da comissão examinadora do exame de qualificação e/ou da defesa desta Dissertação. Meus sinceros agradecimentos pelas críticas, comentários e sugestões que ajudaram a compor e melhorar este trabalho.

Ao Laboratório Sismológico da UFRN – LabSis, na pessoa do coordenador Prof. Dr. Aderson Farias do Nascimento pela colaboração e estrutura física disponibilizada.

Ao Departamento de Geofísica da Universidade Federal do Rio Grande do Norte – DGEF pela estrutura física disponibilizada. Aos funcionários Nayan Lima, Huganisa e Geraldo pela assistência dedicada.

À minha família por toda compreensão e incentivo para que este trabalho pudesse ser realizado. Agradeço ao Od pelo companheirismo e incentivo.

Aos amigos de toda vida, ora mais presentes, ora mais distantes, mas sempre amigos. Às minhas amigas Alany, Rayane Carla e Marília Rodrigues por todo o carinho e cumplicidade.

Por fim, e não menos importante, a todos que de alguma maneira contribuíram para a realização desta Dissertação.

# Resumo

A Faixa Seridó (**FS**) é um cinturão de rochas metassedimentares localizado na Província Borborema (NE do Brasil). Ela foi deformada e metamorfizada no contexto da Orogênese Pan-Africana/Brasiliana. Neste evento tectônico, a crosta foi parcialmente fundida, particularmente na conexão da zona de cisalhamento Patos com a **FS**, alterando suas propriedades reológicas e, consequentemente, sua deformação. O domo anatético de Santa Luzia (~ 575 Ma) se destaca dentre as ocorrências de rochas associadas à fusão parcial. O mapa aeromagnético da **FS** mostra uma expressiva anomalia regional de longo comprimento de onda (> 25 km) em sua porção centro-sul. Esta anomalia apresenta forma sigmoidal e seu eixo central rotaciona de NNE-SSW para E-W próximo a zona de cisalhamento Patos. Anomalias de curto comprimento (< 25 km) e de grande amplitude (até 2.200 nT) se sobrepõem a anomalia regional. Os limites das anomalias magnéticas, frequentemente, coincidem com zonas de cisalhamento regionais, revelando que estas estruturas exercem importante controle tectono-estrutural sobre as fontes das anomalias. A comparação com dados gravimétricos evidencia que ambos os tipos de anomalias compartilham das mesmas fontes anômalas, sendo estas mais magnéticas e menos densas que a crosta circundante. Por outro lado, a correlação com a geologia de superfície mostra que as anomalias geofísicas muitas vezes ocorrem associadas com migmatitos e granitos ricos em magnetita. Nós realizamos duas abordagens de modelagem para os dados geofísicos: a primeira foi uma inversão automática 3D dos dados magnéticos e a segunda foi uma modelagem conjunta 2.5D, guiada pelo interprete, dos dados magnéticos e gravimétricos ao longo de três perfis. Como resultado da análise integrada dos dados geofísicos e geológicos e da modelagem, nós evidenciamos a existência de uma estrutura dômica regional na porção centro-sul da **FS**. Este domo gnáissico em grande escala é

composto por quatro estruturas internas alongadas, geofisicamente modeladas como quatro corpos anômalos, além do material circundante. Em conjunto, eles formam uma estrutura crustal com eixo principal na direção NE-SW que rotaciona para E-W, seguindo a zona de cisalhamento Patos. O domo de Santa Luzia é apenas um domo local em pequena escala dessa estrutura. Os metassedimentos do Grupo Seridó ocorrem em sinformes em torno das estruturas que compõem o domo regional. Em particular, devido ao notável papel da zona de cisalhamento Patos na formação da grande estrutura crustal, é reforçada a concepção de que este lineamento foi um limite tectônico importante durante a Orogênese Pan-Africana/Brasiliana.

**Palavras-chave:** Província Borborema; Faixa Seridó; Zona de cisalhamento Patos; Domo gnáissico; Modelo geofísico.

# *Abstract*

The Seridó Belt (**SB**) is a Neoproterozoic schist belt in Borborema Province, northeast Brazil. It was deformed and metamorphosed in the context of the Pan-African/Brasiliano orogeny. During this tectonic event, the crust was partially melted, particularly at the connection between the Patos shear zone and **SB**, thus altering its rheological properties and, consequently, influencing its deformation. Among the occurrences of rocks associated with partial melting, the Santa Luzia anatetic dome (c. 575 Ma) is particularly noteworthy. The aeromagnetic map of **SB** shows an expressive long-wavelength (>25 km) regional anomaly in the south-central part of the area. This anomaly is sigmoidal in shape and its central axis rotates from NNE-SSW to E-W near the Patos shear zone. Local anomalies with small wavelengths (<25 km) and large amplitudes (up to 2200 nT) overlap this regional anomaly. The limits of the magnetic anomalies often coincide with regional shear zones, thus revealing that the shear zones exert important tectono-structural control on the anomaly sources. Comparison with gravity data shows that both types of anomalies share the same common anomalous sources, being more magnetic and less dense than the surrounding crust. On the other hand, correlation with surface geology shows that the geophysical anomalies often occur in association within homogeneous magnetite-bearing migmatites and granites. We adopted two modelling approaches to analyse the available geophysical datasets. First, a three-dimensional (3D) automatic constrained inversion of the magnetic data was performed and, second, a two-and-a-half-dimensional (2.5D) interpreter-guided joint model was constructed based on magnetic and gravity datasets from three profiles. Through this work, we show the existence of a regional domical structure in the south-central part of **SB**. This large-scale gneiss dome is composed of four elongated internal structures, geophysically modelled as four anomalous bodies,

besides the surrounding material. Together, these form a crustal structure with a long axis in the NE-SW direction that rotates to the E-W direction following the Patos shear zone. The Santa Luzia dome is a local small-scale example of this crustal-scale structure. The metasediments of the Seridó Group occur along synforms surrounding the internal structures that form the regional dome. In particular, because of the remarkable role of the Patos shear zone in shaping this crustal dome, the conception that the Patos shear zone was a very important tectonic constraint during the Pan-African/Brasiliano orogeny.

**Keywords:** Borborema Province; Seridó Belt; Patos shear zone; gneiss dome; geophysical model.

# Sumário

# Capítulo 1 – Introdução

## 1.1. Apresentação

Esta Dissertação é parte dos requisitos necessários para obtenção do título de Mestre em Geodinâmica e Geofísica - área de concentração Geofísica, pelo Programa de Pós-Graduação em Geodinâmica e Geofísica (PPGG), da Universidade Federal do Rio Grande do Norte (UFRN). As atividades relacionadas a este Mestrado estiveram sob orientação do Prof. Dr. Walter Eugênio de Medeiros, membro do PPGG e do departamento de Geofísica da UFRN, e coorientação do Dr. Roberto Gusmão de Oliveira, do Serviço Geológico do Brasil - CPRM.

## 1.2. Contextualização do trabalho

Durante uma orogênese, comumente a crosta continental profunda experimenta fusão parcial devido ao aumento de espessura (e.g. Nelson et al., 1996, Jamieson et al., 2011). A presença do material parcialmente fundido produz mudanças reológicas na crosta influenciando na concentração da deformação e na atuação dos processos orogênicos. A expressiva ocorrência de fusão parcial em orógenos pode ocasionar a extrusão vertical ou ascensão diapírica do material parcialmente fundido e formar domos gnáissicos. Por esse motivo, o estudo de domos gnáissicos traz importantes avanços para o entendimento das orogêneses (Whitney et al., 2004).

A Faixa Seridó (Jardim de Sá, 1994), localizada na extremidade nordeste da Província Borborema (Almeida et al., 1981), foi deformada e metamorfizada no final do Neoproterozoico, no ápice da Orogênese Pan-Africana/Brasiliana. Durante este evento tectônico, a crosta foi parcialmente fundida, particularmente na conexão da zona de cisalhamento Patos com a Faixa Seridó (Corsini et al., 1991), alterando significativamente

suas propriedades reológicas e, consequentemente, influenciando em sua deformação (Tommasi et al., 1995). O domo anatético de Santa Luzia (Archanjo et al., 2013) é um dos exemplos de ocorrência de rochas associadas com a fusão parcial desta orogênese.

O mapa aeromagnético da Faixa Seridó apresenta uma expressiva anomalia regional de longo comprimento de onda (> 25 km) na porção centro-sul da área. Esta anomalia tem forma sigmoidal e seu eixo central muda de NNE-SSW para E-W, próximo à zona de cisalhamento Patos. Anomalias locais de menor comprimento de onda (< 25 km) e de grande amplitude (2.200 nT) ocorrem sobrepostas à anomalia regional. Os limites das anomalias magnéticas muitas vezes coincidem com zonas de cisalhamento regionais, indicando que estas estruturas exercem importante controle tectono-estrutural sobre as fontes das anomalias. A correlação com a geologia de superfície sugere que as fontes das anomalias são dominantemente compostas por migmatitos e granitos ricos em magnetitas resultantes da fusão parcial das rochas do embasamento e da injeção magmática ocorridas durante o Ediacarano.

Moreira et al. (1989) foram os primeiros a interpretar a anomalia magnética de longo comprimento de onda correlacionada à porção central da Faixa Seridó, a partir de dados magnéticos de baixa resolução disponíveis à época. Estes autores propuseram a presença de uma placa máfica magnética localizada na base da crosta superior e a presença de granitos ricos em magnetita nas porções mais rasas da crosta como possíveis fontes causadoras da anomalia.

A geologia de superfície da Faixa Seridó é bem conhecida. Entretanto, a compreensão de sua estrutura profunda tem sido limitada pela ausência de dados geofísicos que permitam interpretações mais detalhadas.

O objetivo geral desta Dissertação é aprofundar o conhecimento geofísico da Faixa Seridó com base na análise qualitativa e quantitativa de novos dados geofísicos,

principalmente gravimétricos e aeromagnetométricos, para explicar a configuração atual e a evolução dos processos crustais ocorridos ao longo de sua história geológica. Os dados geofísicos empregados apresentam melhor resolução quando comparados aos conjuntos de dados anteriormente disponíveis. Por essa razão, eles revelam com maior nitidez os subdomínios e estruturas da Faixa Seridó e de seu embasamento. Especificamente, considerando que a geometria profunda das zonas afetadas por fusão parcial no contexto da Orogênese Pan-Africana/Brasiliana na Faixa Seridó e a das suas estruturas dômicas gnáissicas-migmatíticas resultantes não são bem compreendidas, esta Dissertação apresenta uma interpretação crustal regional para estas estruturas a partir da modelagem de dados aeromagnéticos e gravimétricos recentes.

## 1.3. Localização da área e vias de acesso

A área de estudo está inserida nas porções sul e norte, respectivamente, dos estados do Rio Grande do Norte e da Paraíba, Nordeste do Brasil. A região possui, aproximadamente, 40.400 km² e está localizada entre os meridianos e paralelos 35º20'W a 37º80'W e 5º50'S a 7º30'S.

O acesso ao norte da área de estudo se faz pela BR-226, partindo da cidade de Natal-RN e percorrendo cerca de 185 km até a cidade de Currais Novos-RN. A partir desta cidade é possível acessar as demais localidades da área por outras rodovias (Figura 1).

## 1.4. Materiais e métodos

Os principais materiais utilizados envolvem: (i) **dados aerogamaespectrométricos e aeromagnéticos**: resultantes da compilação de dois levantamentos aerogeofisicos cedidos pelo Serviço Geológico do Brasil – CPRM (Figura

2 e Tabela 1). A base de dados é composta por perfis com linhas de voo e de controle espaçadas de 500 m e 5000 m, orientadas nas direções N-S e E-W, respectivamente, e altura de voo fixada em 100 m sobre a superfície do terreno;

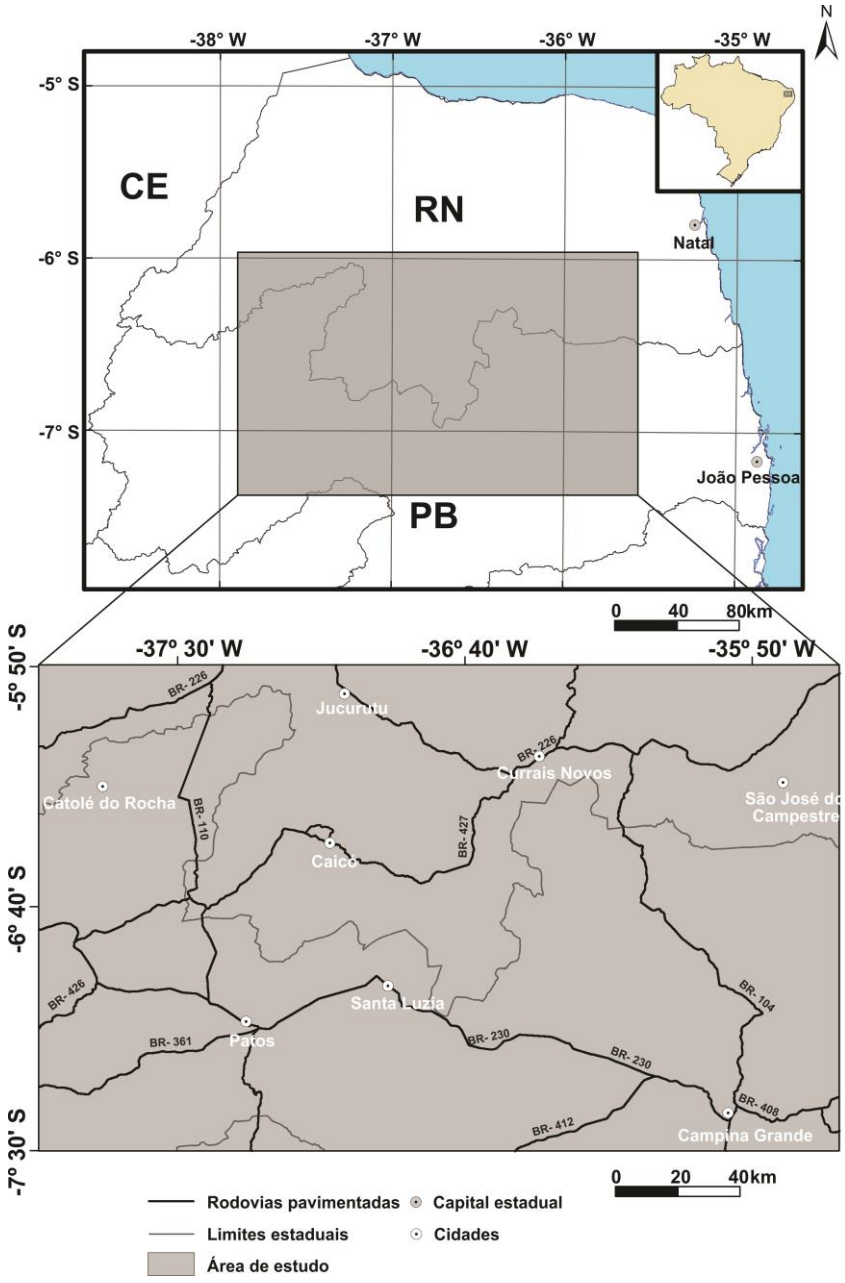


Figura 1 - Mapa de localização da área de estudo (polígono cinza) com as principais vias de acesso.

(ii) **dados gravimétricos terrestres**: levantados entre março de 2013 e dezembro de 2015 para o projeto Províncias Metalogenéticas do Brasil: área RN-PB da CPRM (Figura 3 e Tabela 1). Também engloba dados gravimétricos pré-existentes compilados por Oliveira (2008), integrando levantamentos realizados por diversas instituições (Figura 3 e Tabela 1); (iii) **dados de densidade e de susceptibilidade magnética**: obtidos em testemunhos do furo de sondagem FD-SE-001-Riacho Fechado, Currais Novos-RN (1200 m), contratado pela CPRM; (iv) outros dados geofísicos e geológicos disponíveis na literatura.

| ***Dados Geofísicos*** | | |
|---|---|---|
| ***Aerogamaespectrométricos e aeromagnéticos*** | | |
| **Origem** | **Referências** | ***Observações*** |
| Projeto Levantamento Aerogeofísico Borda Leste do Planalto da Borborema (CPRM) | LASA S.A. & Prospectors (2008) | Espaçamento linhas de voo - 500m (N-S); espaçamento linhas de controle - 5000m (E-W); altura do voo - 100m sobre o terreno |
| Projeto Levantamento Aerogeofísico Paraíba - Rio Grande do Norte (CPRM) | LASA S.A. & Prospectors (2010) | |
| ***Gravimétricos*** | | |
| **Origem** | **Referências** | **Observações** |
| Projeto Províncias Metalogenéticas do Brasil: área RN-PB (CPRM) | Domingos et al. (2017) | Aquisição entre março de 2013 e dezembro de 2015 (3114 estações); pontos distribuídos ao longo de estradas; espaçamento médio de 2km |
| Banco de dados gravimétricos compilados por Oliveira (2008) | Oliveira (2008) | Levantamentos realizados por diversas instituições (UFRN, UFPA, UFPE, USP, CPRM-DNPM-ON, IBGE, PETROBRAS, ANP) |

Tabela 1 – Discriminação dos dados aerogeofísicos e gravimétricos utilizados no trabalho.

Os procedimentos de interpolação, transformações de campo, filtragem e modelagem dos dados geofísicos foram realizados através do *software Oasis Montaj*, da *Geosoft*®. Cada etapa é resultado de vários testes, sendo escolhido o mais adequado.

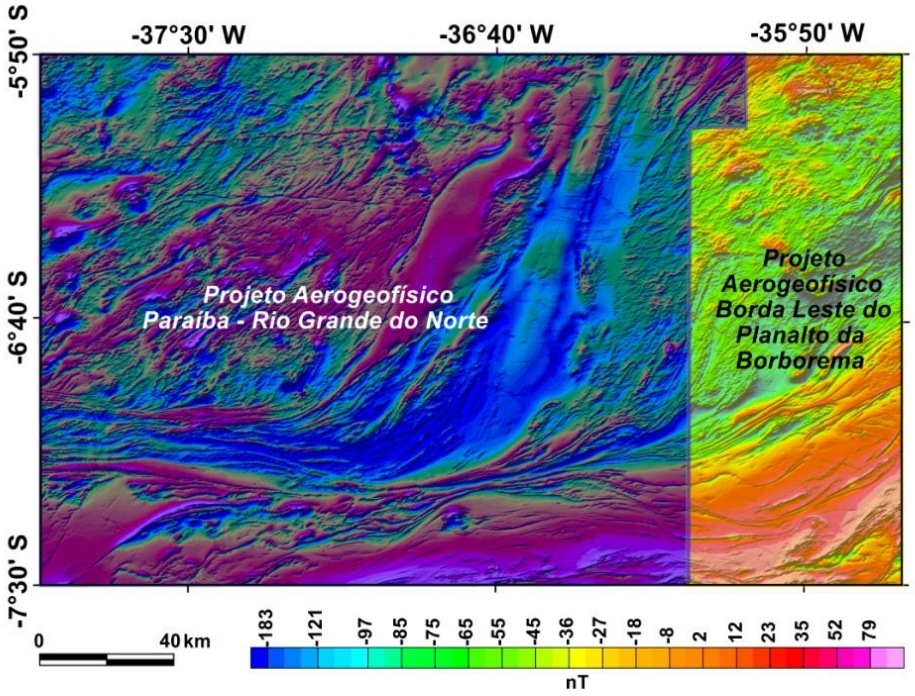


Figura 2 - Anomalia do campo magnético total da área de estudo após a remoção do IGRF (*Internacional Geomagnetic Reference Field)* com sobreposição das áreas dos respectivos projetos aerogeofísicos utilizados (Paraíba - Rio Grande do Norte e Borda Leste do Planalto da Borborema).

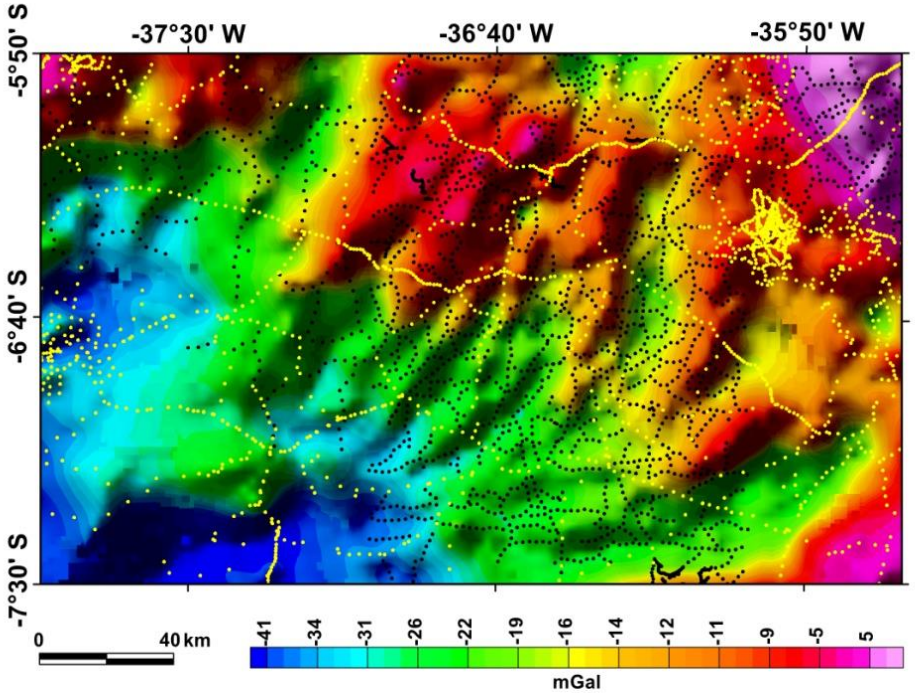


Figura 3 - Anomalia Bouguer da área de estudo com distribuição das estações gravimétricas utilizadas conforme Oliveira (2008) (pontos amarelos) e estações levantadas entre 2013 e 2015 pela CPRM (pontos pretos).

Para os dados aeromagnéticos, a redução ao polo (Blakely, 1995) e a separação em componentes regional e residual pelo método de Spector & Grant (1970) foram realizadas. Por outro lado, foi empregado o método de separação por ajuste polinomial robusto proposto por Beltrão et al. (1991) para a separação das anomalias causadas por fontes rasas e profundas da anomalia Bouguer.

A modelagem dos dados geofísicos foi realizada através de duas abordagens executadas de maneira independente. A primeira envolveu a inversão automática tridimensional do vetor magnetização a partir dos dados aeromagnéticos (Ellis et al., 2012; MacLeod & Ellis, 2013; MacLeod & Ellis, 2016). A segunda compreendeu a modelagem conjunta 2.5D dos dados gravimétricos e magnéticos, guiada pelo usuário e com base no algoritmo de modelagem descrito por Talwani et al. (1959).

## 1.5. Estrutura da Dissertação

Esta Dissertação é apresentada sob a forma de artigo científico e está dividida em três capítulos. Após este capítulo introdutório, o Capítulo 2 apresenta o manuscrito intitulado "*Geophysical evidence of doming during the Pan-African/Brasiliano orogeny in the Seridó Belt, Borborema Province, Brazil"*, submetido ao periódico *Precambrian Research*. O Capítulo 3, "Considerações finais" consiste de uma síntese dos principais resultados e implicações desse estudo. Além disso, apresenta recomendações para trabalhos futuros.

# Capítulo 2 - Manuscrito submetido: “*Geophysical evidence of doming during the Pan-African/Brasiliano orogeny in the Seridó Belt, Borborema Province, Brazil”*

---

Manuscrito submetido à revista *Precambrian Research*.

# GEOPHYSICAL EVIDENCE OF DOMING DURING THE PAN-AFRICAN/BRASILIANO OROGENY IN THE SERIDÓ BELT, BORBOREMA PROVINCE, BRAZIL

Nitzschia R. R. Domingos[(1),(2)] , Walter E. Medeiros[(2)*] and Roberto G. Oliveira[(1)]

(1) CPRM-Geological Survey of Brazil

Av. Sul, 2291, Afogados, Recife/PE, Brazil, CEP: 50770-011.

E-mail: nitzschia.domingos@cprm.gov.br, roberto.gusmao@cprm.gov.br

(2) Geophysics Department and Pos-graduate Course on Geodynamics and Geophysics – Federal University of Rio Grande do Norte (UFRN). Campus Universitário Central, Natal/RN, Brazil, CEP: 59078-970.

E-mail: walter.ufrn@gmail.com

*Corresponding author. Phone: +55 84 999887571

## ABSTRACT

The Seridó Belt (**SB**) is a Neoproterozoic schist belt located in the Borborema Province, Brazil. It was deformed and metamorphosed in the Pan-African/Brasiliano orogeny during the West Gondwana agglutination. Associated with the orogeny, intense partial melting occurred (e.g. the Santa Luzia anatetic dome). The aeromagnetic map of **SB** shows a long-wavelength anomaly with sigmoidal shape, whose limits coincide with shear zones. In particular, the central axis of the anomaly rotates from NNE-SSW to W near the Patos shear zone. Comparison with gravity data shows that both types of anomalies share common sources, which are rocks more magnetic and less dense than the surrounding crust. Correlation with surface geology shows that the geophysical anomalies are associated with magnetite-bearing migmatites and granites resulted from the partial melting. We adopted two modelling approaches to analyse the geophysical datasets. First, a three-dimensional automatic inversion of the magnetic data was performed and, second, a two-and-a-half-dimensional interpreter-guided joint modelling of magnetic and gravity datasets was done, where we also utilised estimates of susceptibility and density measured in cores from a stratigraphic borehole. Both model outputs were consistent and, as a result, we characterize a regional domical structure in the south-central part of **SB**. This large-scale crustal dome is composed of four elongated internal structures, which were geophysically modelled as four anomalous bodies. Together, they form a crustal structure with a long axis in the NE-SW direction that rotates to the E-W direction after the Patos shear zone. The anomalous bodies are the geophysical expressions of rock volumes where the material resulting from the partial melting are concentrated. The Santa Luzia anatetic dome is a local small-scale part of this large structure. The formation of this crustal-scale dome is associated with the Pan-African/Brasiliano orogeny, thus evidencing that intense deformation was concentrated in this region. In particular, because the Patos shear zone has a key role in shaping this crustal

dome, the conception that this shear zone was a very important tectonic constraint during the orogeny is strongly supported.

**Keywords:** Borborema Province; Seridó Belt; Patos shear zone; gneiss dome; geophysical model.

## 1. INTRODUCTION

Gneiss domes (Eskola, 1949) are common structures in exhumed orogens (Teyssier and Whitney, 2002; Whitney et al., 2004). They can occur under compressive, strike-slip or even extensive tectonic settings and suggest vertical movements in the crust (Brun, 1983). Often, gneiss domes are associated with tectonic boundaries in collisional orogens and possibly to suture zones in accretionary orogens (Baldim and Oliveira, 2016). They are formed by a core of metamorphic-plutonic rocks (migmatites ± granitoids) that can display a low-pressure (4–6 kb)–high-temperature (500–700 °C) metamorphic rock assembly (Dixon, 1987; Whitney et al., 2004). Their cores are surrounded by a mantle of supracrustal units (e.g. quartzites, marbles, metapelites and metaconglomerates). Their core and mantle might be exposed depending on the degree of denudation and weathering processes. These structures are also known as mantled gneiss domes, granite-gneiss domes, metamorphic domes and migmatite domes (Whitney et al., 2004). They are often anatetic migmatite domes because partial melting is usually a key process in their formation (Teyssier and Whitney, 2002; Whitney et al., 2004).

Well-documented examples of gneiss domes of different ages occur in the Himalaya (e.g. Zhang et al., 2017), Appalachian orogen (e.g. Zietz et al., 1980) and the Variscan belt in Spain (e.g. Ayarza and Martínez Catalán, 2007). In particular, gneiss domes of Precambrian age are reported in Brazil in the São Francisco craton (e.g. Cutts et al., 2019), southern Amazonian craton (e.g. Rizzotto et al., 2019), and in the southern part of the Borborema Province (**BP**) (e.g. D'el-Rey Silva, 1995).

Gneiss dome formation processes remain unclear, with the following mechanisms being proposed: (i) the rising of hot orogenic crust (Eskola, 1949; Fletcher, 1972; Soula, 1982); (ii) complex fold interferences (Talbot, 1974; Yin, 2004); (iii) duplex-related antiforms (Brown et al., 1986); (iv) crustal extension (Vanderhaeghe et al., 1999); and (v) a

combination of lower crustal contraction and upper crustal extension (Crowley et al., 2001). However, several similarities are observed between gneiss domes, regardless of the tectonic context and the processes involved in their formation. Gneiss domes are circular-to-elliptical in shape and occur in linear strips parallel to the main direction of the associated orogen (Whitney et al., 2004). Usually, the largest dome dimension ranges from tens to hundreds of kilometres and the smallest dimension from ten to twenty kilometres (Dixon, 1987). Often, gneiss domes are formed by clusters of small domes, articulated as secondary structures of a large domical structure (e.g. the Thor-Odin dome, see Vanderhaeghe et al. 1999, and the Lugo dome, see Martínez Catalán et al., 2018). The smaller structures are commonly distributed in *en echelon* pattern (Dixon, 1987) and are separated by synclines from the supracrustal rocks surrounding their core (Dixon, 1987; Zhang et al., 2017). During dome formation, the development of large-scale folds is common (Dixon, 1987). In addition, dome boundaries are often defined by shear zones (e.g. Zang et al., 2017), whilst the contacts between the core and mantle rocks usually form unconformities (Dixon, 1987).

In active orogens, the extrusion of partially melted layers (i.e. hot migmatites and leucogranites) of mid-crustal rocks (bounded by ductile shear) and dome formation are common events (e.g. Jamieson et al., 2006; Searle and Treloar, 2019). As a result, tectonics, metamorphism, crust deformation and crust/mantle interaction can be jointly explained (Grujic, 2006).

From a geophysical viewpoint, the mantle of supracrustal rocks commonly presents a positive density contrast (0.1–0.5 g/cm$^3$) in relation to the core of metamorphic-plutonic rocks due to the fact that the core usually has a relatively more mafic and/or aluminous composition (Fletcher, 1972; Soula et al., 2001). As a consequence, negative gravity anomalies are usually associated with the central part of gneiss domes (e.g. Kodama and Chapin, 1984; Ayarza and Martínez Catalán, 2007). On the other hand, the core of

98 metamorphic-plutonic rocks commonly includes magnetite-bearing rocks of magmatic
99 origin, usually leading to strong positive contrasts in susceptibility. As a result, gneiss domes
100 are often associated with expressive regional magnetic anomalies (e.g. Ayarza and Martínez
101 Catalán, 2007; Martínez Catalán et al., 2018).

102 The interpretation of gneiss domes might offer important contributions to the
103 understanding of orogenesis. For example, in exhumed orogens, the occurrence of
104 inhomogeneous migmatites and granites inside the core suggests that the doming process of
105 the middle crust is closely linked to the partial melting and flow of partially melted materials
106 within the orogen (Whitney et al., 2004). Therefore, these structures are relevant for
107 understanding the thermal, chemical, and mechanical evolution of the continents (Teyssier
108 and Whitney, 2002; Kruckenberg et al., 2011). For example, in the active Himalayan orogen,
109 migmatites and granites reveal when and where the crust has been melted since the onset of
110 the India–Asia collision (Jamieson et al., 2011).

111 Borborema Province, located in northeastern Brazil (Fig. 1a), is an orogenic domain
112 that was formed during the Pan-African/Brasiliano Neoproterozoic orogeny (Ganade de
113 Araújo et al., 2014). Some gneiss domes have been identified in **BP** by Whitney et al. (2004),
114 including the Itabaiana dome (D'el-Rey Silva, 1995), the Jirau do Ponciano and Simão Dias
115 domes (D'el-Rey Silva, 1995), Paleoproterozoic domes in the Sergipano Belt (D'el -Rey
116 Silva, 1995; Oliveira et al., 2015).

117 In the Seridó Belt (**SB**) (Fig. 1b and Fig. 2), which is an important tectonic subdomain
118 of Borborema Province, local domical structures have been discussed by Dantas (1992) and
119 Magini et al. (1997). These authors point out the existence of gneissic-granitic local domical
120 structures, forming elliptical cores bordered by metasediments in the midwest part of **SB**. In
121 addition, Archanjo et al. (2013) defined the Santa Luzia local anatetic dome at the connection
122 with the Patos shear zone (PSZ in Fig. 1). This dome shows an exposure of migmatites

generated by the partial melting of the crust during the Neoproterozoic Pan-African/Brasiliano orogeny. However, considering that the deep-rooted geometry of the small-scale gneiss domes in **SB** is not well understood, we present an interpretation of these structures in a regional context using geophysical data. We use recent high-resolution aeromagnetic, aerogamaspectrometric and gravity data alongside density and magnetic susceptibility measurements of cores from a stratigraphic borehole to interpret and model the deep structures of **SB**. In doing so, we provide evidence of the existence of a regional domical structure in the south-central part of **SB**, thus revealing that intense deformation was concentrated in this region during the Pan-African/Brasiliano orogeny.

## 2. MATERIALS AND METHODS

### 2.1 Geological setting

*2.1.1 Borborema Province*

Borborema Province (Almeida et al., 1981) in northeastern Brazil (Fig. 1a) is a key region for understanding West Gondwana amalgamation (Fig. 1a) because it represents part of the orogen located between the São Francisco–Congo and West African cratons (Brito Neves and Cordani, 1991; Trompette, 1997). The **BP** is composed of Archean–Paleoproterozoic basement blocks surrounded by Neoproterozoic metasedimentary belts (Van Schmus et al., 1995; Brito Neves et al., 2000; Ganade de Araújo et al., 2014). Internally, an expressive set of interconnected shear zones compartmentalises the **BP**. Its evolution extended from the Archean to the Phanerozoic, and its current structural framework dates from the end of the Pan-African/Brasiliano orogeny (700–500 Ma). During the early Neoproterozoic, magmatism and sedimentation occurred in the central part of the **BP** (Van Schmus et al., 1995) and, in the middle-to-late-Neoproterozoic, a large volume of granite rocks was emplaced (Sial, 1986; Neves et al., 2000). Granitoid emplacement is spatially related to the

148 interconnected system of the BP shear zone (Caby et al., 1991; Corsini et al., 1991; Vauchez
149 et al., 1995; Neves et al., 2000; Cavalcante et al., 2016).

150 Van Schmus et al. (1995) compartmentalised the **BP** into three subprovinces (Fig.
151 1a), namely the Northern, Transversal (limited by the Patos and Pernambuco shear zones)
152 and Southern subprovinces. This division is corroborated by the analysis of regional gravity
153 and aeromagnetic data performed by Oliveira and Medeiros (2018).

154 The orogenic events that produced the **BP** tectonic framework resulted from the
155 convergence of the West African-São Luis craton and the São Francisco-Congo craton in the
156 context of the West Gondwana amalgamation (Brito Neves and Cordani, 1991; Trompette,
157 1994, 1997; Tohver et al., 2006; Li et al., 2008). According to Ganade de Araújo et al.
158 (2014), the Pan-African/Brasiliano orogenesis begun with the collision of the **BP** with the
159 West African-São Luis craton to the west (at c. 620–610 Ma) followed by the collision with
160 the São Francisco-Congo craton to the south (at c. 590–580 Ma). The deformation resulting
161 from the interaction between these two events between 590 Ma and 570 Ma enabled the
162 formation of a large system of transcurrent shear zones (Tommasi et al., 1995; Vauchez et
163 al., 1995) in a tectonic regime producing a general extrusion (or tectonic escape) to the
164 northeast (Brito Neves et al., 2000; Alkmim et al., 2001; Ganade de Araújo et al., 2014).
165 This tectonic regime was associated with extensive magmatism in the **BP**.

166 The peak of deformation, magmatism and metamorphism caused by the Pan-
167 African/Brasiliano orogeny is assumed to have occurred at approximately 600 Ma (Brito
168 Neves et al., 2014). Metamorphism of the Ediacaran sediments and thrust deformation—
169 including nappes formation in the northwestern **BP** region (Caby and Arthaud, 1986; Caby
170 et al., 1991) and at the northern edge of the São Francisco craton (D'el-Rey Silva, 1995;
171 Caxito et al., 2016)—preceded the formation of shear zones and/or the reactivation of pre-
172 existing structures (Oliveira and Medeiros, 2018).

*2.1.2 Patos shear zone*

The Patos shear zone (PSZ) is a long E-W trending dextral strike-slip shear zone that limits the Northern and Transversal subprovinces of the **BP** (Figs. 1a, 1b and 2). Migmatites and high-temperature gneiss mylonites occur in the western sector of the Patos shear zone (Vauchez et al., 1995; Corsini et al., 1998; Cavalcante et al., 2016). In the eastern sector, strain transfer is assumed to have occurred from the Patos shear zone to **SB** (the Patos–Seridó system) through the shear zone set that agglutinated in the Patos shear zone (Corsini et al., 1991; Tommasi et al., 1995).

In the central and eastern parts of the Patos–Seridó system, the occurrence of migmatites (e.g. Archanjo et al., 2013; Viegas et al., 2014) associated with granite emplacement (Corsini et al., 1991; Cavalcante et al., 2016) suggests that intense partial melting occurred in this region. Cavalcante et al. (2016) proposed that the Patos shear zone probably functioned as a corridor for efficient vertical melt migration in the region of the Espinho Branco anatexite (Viegas et al., 2014). In addition, according to Cavalcante et al. (2016), magmatism and partial melting events occurred for approximately 25 Ma simultaneously with the high-temperature–low-pressure metamorphism characterised by Archanjo et al. (2013).

Corsini et al. (1998) concluded that along the Patos shear zone, temperatures exceeded 700 °C regionally and reworked both the basement and proterozoic covers. These authors characterised the thermal history of the Patos shear zone area as consisting of a slow cooling between 580 and 500 Ma (due to the occurrence of large amounts of high-temperature mylonites and migmatites) followed by faster cooling at approximately 500 Ma that was associated with rapid uplift and erosion.

Brito Neves et al. (2016) established the presence of a continental magmatic arc (at c. 635–580 Ma) in the northern part of the Tranversal Zone (Fig. 1a). In this context, they

198 proposed that the Patos and Malta shear zones would have functioned as a continental
199 boundary transform (up to 20 km wide and 750 km long), which would have represented the
200 boundary between two plates—one to the north (the Northern Subprovince) and one to the
201 south (the Transversal Subprovince).

202 In accordance with this interpretation, Oliveira and Medeiros (2012), Luz et al.
203 (2015), and Oliveira and Medeiros (2018) suggest that the crust in the north of the Patos
204 shear zone has different geophysical characteristics to the crust in the south of this shear
205 zone, emphasising that the Patos shear zone separates different lithospheric domains. From
206 this perspective, by interpreting gravity and magnetic data in the north of the Patos shear
207 zone, Oliveira and Medeiros (2018) proposed the existence of the Granjeiro-Seridó
208 Subdomain. As additional support to the existence this subdomain, Hollanda et al. (2015)
209 described the equivalent age and stratigraphy of two metasedimentary sequences, one
210 pertaining to the Lavras da Mangabeira belt and the other to **SB**, which are geographically
211 distant but show common structural control of the Patos shear zone.

212 *2.1.3 Seridó Belt*

213 The Seridó Belt is oriented in the NNE-SSW direction and is composed of
214 Neoproterozoic metasedimentary rocks (Seridó Group) that were originally deposited in a
215 platform-to-turbiditic environment (Van Schmus et al., 2003) over the Archean–
216 Paleoproterozoic basement of the Rio Piranhas-Seridó Domain (Fig 1b). This basement is
217 mainly composed of gneissic-migmatitic rocks of the Caicó Complex (Souza et al., 2016).
218 Locally and without a well-defined spatial distribution, Archean rocks also occur (Souza et
219 al., 2016). The Neoproterozoic sequence of the Seridó Group is formed, from the bottom to
220 the top, by paragneisses, marbles, iron formation, and metaultramaphic rocks of the Jucurutu
221 Formation, quartzites and metaconglomerates of the Equador Formation, and mica schists
222 of the Seridó Formation (Jardim de Sá, 1994). Van Schmus et al. (2003) established a U–Pb

223 age of 0.65 ± 0.05 Ga for the maximum depositional age of the Seridó and Jucurutu
224 Formations.

225 The eastern limit of **SB** is defined by the Picuí-João Câmara shear zone, which
226 separates the Rio Piranhas-Seridó Domain from the São José do Campestre Domain (Fig.
227 1b). The latter domain consists predominantly of Paleoproterozoic and Archean rocks,
228 Neoproterozoic granites and allochthonous supracrustal granites of the Seridó Group
229 (Dantas, 1997). The western and south limits are defined by the Portalegre and Patos shear
230 zones. To the north, Cretaceous and recent sedimentary deposits occur.

231 In **SB**, regional metamorphism occurred under conditions of high temperature and
232 low pressure associated with a dextral transpressive deformation at c. 575 Ma (Archanjo et
233 al., 2013). Lima (1987) measured temperatures below 500 °C and pressures of approximately
234 3 kbar in the western part of the study area whilst, in the central part, he measured
235 temperatures of up to 620 °C and pressures of 4 kbar (amphibolite facies).

236 *2.1.4 Santa Luzia dome*

237 The Santa Luzia dome was defined by Archanjo et al. (2013) as an exposition of
238 Neoproterozoic migmatitic rocks, the limit of which is represented by the red line in Fig. 2.
239 The dome structure has a NE-SW orientation and is located at the connection between the
240 Patos shear zone and **SB** in the region where it is assumed that stress transfer occurred.
241 Archanjo et al. (2013) pointed out that anatexites are the result of partial melting of pre-
242 existing basement rocks (Fig. 3a). In the exposition of the migmatitic rocks, remains of
243 protoliths from the basement are often found (Figs. 3b and 3c), although homogeneous
244 equigranular leucogranites can also be observed (Figs. 3c and 3d). Archanjo et al. (2013)
245 estimated U-Pb ages in zircons (from the migmatite felsic neosome) of approximately 575
246 ± 3.4 Ma and interpreted the timing of the high-temperature deformational event in **SB** at c.
247 575 Ma. From the observation of outcrops, Archanjo et al. (2013) suggested that partially

melted rocks exploited the contact between the Seridó Group and the basement rocks to form the dome structure. However, these authors make no consideration of the melt ascension mechanism or the doming process in the migmatitic rocks. Metasediments of the Seridó Group occur to the east and west of the Santa Luzia dome (Figs. 3e and 3f) in a similar manner to the domes described by Dixon (1987) and Zhang et al. (2017). At the western limit, we observed quartzites of the Equador Formation (Fig. 3e) that outcrop with a dip of 50º/287º Az. We found no evidence of relative displacement between the quartzite layers, so that we interpret this dip as being compatible with the flank of a domical structure. At the eastern limit, the metasediments are deformed by the Umburana shear zone.

Archanjo et al. (2013) measured magnetic susceptibility values in the range 1 x $10^{-3}$ SI to 55 x $10^{-3}$ SI for the migmatitic rocks located inside the dome. Magnetite is the main element contributing to these high susceptibility values. Archanjo et al. (2013) suggested that the magma emplacement and the shear deformation regime for both the Santa Luzia dome and the Acari granitoid (A in Fig. 2) were contemporaneousness.

## 2.2 Geophysical data

The geophysical database we used was obtained from surveys contracted or performed by the Geological Survey of Brazil (SGB/CPRM) with the addition gravity datasets from several institutions (for a detailed description of these gravity data, see Oliveira and Medeiros, 2012). In addition, we performed measurements of density and magnetic susceptibility of the cores of SGB/CPRM borehole FD-SE-001 (Fig. 2).

### *2.2.1 Aerogamaspectrometric and aeromagnetic data*

High-resolution aerogamaspectrometric (Fig. 4) and aeromagnetic (Figs 5 e 6) data were acquired during the same surveys (http://geosgb.cprm.gov.br/downloads/) using the same specifications for acquisition, control and flight height lines. Acquisition was carried out

along N-S flight lines spaced at 500 m, whilst the control lines were flown in the E-W direction with line spacing of 5,000 m. The flight height was 100 m above the ground surface. Standard survey corrections were performed by the company contracted for the surveys. For a more detailed description, see the SGB/CPRM website (http://www.cprm.gov.br/aero/aero.htm).

Figure 4 shows the false-colour ternary composition map of potassium (K), equivalent thorium (eTh), and equivalent uranium (eU) channels, with transparency over the topography. Gamma-spectrometric analysis allowed us to establish correlations with surface geology due to the low penetrative energy (30–40 cm in rocks and soils) of the gamma radiation generated by radio-elements K, Th, and U (Minty, 1997).

The aeromagnetic data were interpolated on a 125 × 125 m mesh using the Bigrid method. Figure 5 shows the upward continuation (to 1,000 m) of the anomalous magnetic field that was applied to highlight regional sources (Blakely, 1995). Figure 6 presents the reduced-to-the-pole version of the magnetic anomaly, which was used in the correlation with the other datasets. The radially averaged power spectrum of the reduced-to-the-pole magnetic anomaly (not shown) was calculated using the Spector and Grant method (1970). This was used to estimate in the study area the mean of the top depths of the deepest magnetic sources (approximately 17.5 km). Rocks below this depth are likely to have temperatures above the Curie's temperature (575 °C) and, as such, do not contribute to the magnetic anomalies.

The long-wavelength magnetic anomaly present in **SB** (Fig. 5 and Fig. 6) was first interpreted by Moreira et al. (1989) using the low-resolution magnetic data available at that time. These authors proposed that the magnetic anomaly was the result of two factors: (1) the presence of a magnetic mafic plate emplaced at the base of the upper crust and (2) the presence of magnetite-bearing granites in the shallowest part of the crust. The latter bodies

298 contain pieces of mafic xenoliths with high magnetic susceptibility and are responsible for
299 generating the associated negative gravity anomalies. Moreira et al. (1989) pointed out that
300 the magnetite-rich granites could have been formed by the partial melting of the mafic plate
301 or the mantle itself.

302 *2.2.2 Gravity data*

303 Figure 7 shows the Bouguer anomaly map based on Kriging interpolation over the same grid
304 of the two gravity datasets. One dataset consists of recent data acquired by the SGB/CPRM,
305 with an average spacing of 2,000 m between measurements along roads. The second dataset
306 contains the available regional gravity measurements that have been acquired by several
307 Brazilian research and teaching institutions (Oliveira and Medeiros, 2012). All gravity
308 measurements were corrected according to the International Gravity Standardisation Net-
309 1971 (IGSN-71). In addition, to calculate the Bouguer anomaly, an average density of 2.67
310 g/cm³ for the topographic masses was adopted. The gravity dataset resulting from the
311 combination of the two described datasets was interpolated onto a 2.5 km × 2.5 km mesh.

312 *2.2.3 Magnetic susceptibility and density data*

313 Borehole FD-SE-001 was contracted by SGB/CPRM to obtain detailed subsurface
314 stratigraphic information of the Seridó Group (Medeiros et al., 2017). The borehole reached
315 approximately 1,200 m in depth, and its location is shown in Fig. 2. We performed
316 measurements of magnetic susceptibility and density on the cores obtained from this
317 borehole. Three measurements of these physical properties were taken for each meter of the
318 core. The mean values of these measurements are shown in Fig. 8 as profiles of density
319 ($g/cm^3$) and magnetic susceptibility ($10^{-3}$ SI, on a logarithmic scale), together with the
320 lithological units.

321

## 3. INTEGRATED REGIONAL GEOPHYSICAL AND GEOLOGICAL INTERPRETATION

The red-green-blue (RGB) ternary composition map (K in red, eTh in green and eU in blue) of the aerogamaspectrometric data (Fig. 4) shows excellent correlation with the surface geology (Fig. 2). In particular, high-K content (shades of red) are mainly related to Neoproterozoic granites and pegmatite intrusions. The metasediments of the Seridó Group show enrichment in eU (shades of green). In comparison, ortho-derivative rocks are generally associated with enrichment in the three radio-elements and have whitish tones. This latter pattern of colours occurs very commonly in the south-central part of the study area (Fig. 4). In this region, outcropping **SB** rocks are structurally controlled by the Patos shear zone. The regional configuration of these rocks is controlled by important shear zones; to the east by the Umburana shear zone (USZ) and to the west by the Várzea (VSZ) and Totoró (TSZ) shear zones. In the central part of **SB**, large synforms and structural basins of metasediments of the Seridó Group (shades of blue in Fig. 4) alternate with the basement rocks.

The reduced-to-the-pole magnetic anomaly map (Fig. 6) shows several short-wavelength (<25 km) anomalies in the south-central part of **SB** with amplitudes of up to 2,200 nT. However, at the regional scale, these form a single, pronounced long-wavelength (>25 km) anomaly with a sigmoidal shape, the elongated axis of which is NNE-SSW rotating to E-W near the Patos shear zone. This regional magnetic anomaly shows spatial correlation with the K-, eTh- and eU-enriched rocks that occur in the central region of **SB** (Fig. 4 and Fig. 6). At the surface (see Fig. 2 and Fig. 6 for correlation), their occurrence coincides with inhomogeneous granites (such as the Acari granitoid, represented by A in Fig. 2), basement orthognessic rocks and migmatites (such as the Santa Luzia anatetic dome). The limits of these bodies are well marked by the presence of regional shear zones (Fig. 6), revealing that

these structures exert important tectono-structural control over the sources causing the magnetic anomaly, from shallow-to-deep crustal levels. In particular, the remarkable influence of the Patos shear zone in shaping the magnetic anomaly is notable.

In the Bouguer anomaly map (Fig. 7), gravity alignments in the NNE-SSW direction, which bend to the west, occur in the south-central part of **SB**. Note that the gravity map shows a pattern of alternated positive and negative anomalies; the positive anomalies are generally associated with the presence of metasediments of the Seridó Group as is the case, for example, to the west of the Totoró shear zone (TSZ in Fig. 2 and Fig. 7). The negative anomalies are associated with granites, gneisses and magnetic migmatites. Their limits are commonly structurally controlled by shear zones, such as the Várzea (VSZ), Totoró (TSZ), Umburana (USZ) and Frei Martinho (FMSZ) shear zones in Fig. 7.

Negative Bouguer anomalies (Fig. 7) correlate with short-wavelength magnetic anomalies (Fig. 6) that occur in the south-central part of **SB**. This shows that the sources of the magnetic anomalies are rocks with average densities below the mean value of the crust density in this region. In fact, measurements from the borehole core (Fig. 2 and Fig. 8) show an average density of 2.64 g/cm³ for the basement rocks and high values of magnetic susceptibility (up to $100 \times 10^{-3}$ SI). On the other hand, for the intercepted metasediments of the Seridó Group, the mean density is equal to 2.78 g/cm³ whereas the magnetic susceptibility values are lower than $1 \times 10^{-3}$ SI.

These geophysical characteristics of **SB** are consistent with those described for several gneiss domes around the world. For example, high magnetisation contrasts and negative density contrasts are described by Ayarza and Martínez Catalán (2007) for the Lugo dome located in the Variscan belt in eastern Galicia, North West Spain. The Lugo dome is an antiform structure with its largest axis in the N-S direction. It is formed by inhomogeneous migmatites and granites derived from the partial melting of paragneisses surrounded by low-

grade metasediments. Another example is described by Zhang et al. (2017), who proposed that linear dome-like zones have formed the Tengchong terrain due to deformation during the India–Asia oblique collision during the Cenozoic. In this terrain, deformation is characterised by the formation of large-scale shear zones and regional-scale folds as well as smaller secondary shear zones between antiforms and extensive partial melting and emplacement of granitoid bodies.

Based on the correlation between the geological and geophysical data, we propose the existence of a regional domical structure in the crust of **SB**. In accordance with the described geophysical anomalies, this domical structure is elongated, with its main axis following the direction of the belt (i.e. NNE-SSW rotating to E-W near to the Patos shear zone). This regional domical structure contains several secondary domes, one of them being the Santa Luzia dome. The proposed limits of the regional dome coincide with shear zones given the strong correlation between these structures and the geophysical anomalies. The Umburana (USZ), Várzea (VSZ), and Totoró (TSZ) shear zones correspond to the outcropping limits of the dome (Fig. 2 and Fig. 4).

Note that the magnetic anomaly map in the region between the Totoró (TSZ), Várzea (VSZ) and Umburana (USZ) shear zones (Fig. 6) displays strong signal strength, evidencing the fact that the dome structures are outcropping or lie close to the surface. On the other hand, to the east of the Umburana shear zone (USZ), the presence of metasediments of the Seridó Group (Fig. 2 and Fig. 4) cover the magnetic bodies and attenuate the magnetic signal significantly. This is also observed to the east of the Várzea shear zone (VSZ) and the Santa Luzia dome in the central part of the study area. Denudation and weathering processes in the area have produced an apparent spatial distribution of secondary domes. In the most-uplifted areas, the tops of the domes emerge and in the less-uplifted areas, the tops are covered by metasediments.

## 4. GEOPHYSICAL MODELLING

Based on the qualitative interpretations presented in Section 3, the geophysical data were quantitatively modelled to produce a crustal model for the regional dome. Two approaches were adopted: (1) automatic three-dimensional (3D) constrained inversion, in which only magnetic data was used and (2) two-and-a-half-dimensional (2.5D) user-guided integrated modelling of gravity and magnetic data, in which other geological and geophysical information was also used.

### 4.1 Automatic inversion of magnetic anomalies

We performed a 3D constrained inversion of the magnetisation vector using the aeromagnetic data (Ellis et al., 2012; MacLeod and Ellis 2013; MacLeod and Ellis, 2016). We used the most commonly applied version of this methodology in which the process is automatic (i.e. without user intervention). The inversion model represents the subsurface as voxel cells (volume elements) and a magnetisation vector is assigned to each cell. However, the variation in magnetisation between neighbouring cells is minimised so that the classic smoothness constraint is imposed (Constable et al., 1987; MacLeod and Ellis, 2016). Due to this constraint, the cells presenting anomalous values of magnetisation tend to cluster close to the surface (Silva et al., 2002) resulting in anomalous bodies restricted to a maximum depth of 11 km (a value that is established automatically). As a result, the obtained magnetisation distribution provides an estimate in which the anomalous bodies are as shallow as possible.

A window of the aeromagnetic data (a 122 km × 129 km are indicated by the blank rectangle in Figs. 4 to 7) was chosen for the inversion. Figure 9 shows the estimates obtained for the magnetic susceptibility distribution in this area. In comparison, Fig. 10 shows the fit between the observed (Fig. 10a) and calculated (Fig. 10b) anomalies, with the latter using

422 the anomalous bodies shown in Fig. 9. For a better representation of the anomaly fitting, the
423 observed and calculated magnetic anomalies are shown along the same three profiles (Fig.
424 10c) used in the magnetic and gravity modelling Section 4.2.

425 Note that the estimates of the spatial distribution of magnetic susceptibility shown in
426 Fig. 9 are only associated with the induced component of magnetisation. Although it is
427 possible to obtain the component associated with remnant magnetisation (not shown), this
428 component could be disregarded in the regional modelling context for two reasons. First, the
429 integrated analysis of the observed magnetic anomalies with the geological information
430 shows that the remnant component of magnetisation is strictly associated with small isolated
431 bodies (e.g. dikes and necks associated with volcanic events during the Phanerozoic).
432 Second, the anomalies calculated when only the induced component of the magnetisation
433 was included gave an excellent fitting of the observed anomalies (Fig. 10).

434 The isovalue contours of the magnetic susceptibility distribution are superposed onto
435 the geologic map and the ternary composition (RGB of K, eTh and eU) in Fig. 11 and Fig.
436 12, respectively. A 3D view of Fig. 12 is also shown in Fig. 13, produced using the same
437 crustal sections used in Section 4.2. In turn, the isovalue contours of the magnetic
438 susceptibility distribution are superposed onto the Bouguer gravimetric anomaly in Fig. 14.
439 Figure 11 and Figure 12 show that for the central part of the study area, where granites and
440 migmatites outcrop, the limits of the magnetic susceptibility distribution coincide very well
441 with the contours of shallow and outcropping lithologies (see also the cross-sections in Fig.
442 3). Towards the edges of the study area, where the metasediments of the Seridó Formation
443 outcrop expressively (Fig. 2), the magnetic susceptibility contours indicate the existence of
444 subsurface magnetic bodies (Fig. 11). In regions where magnetic bodies are not outcropping
445 (e.g. in the southeastern part of the area in Fig. 11), antiform structures have been mapped
446 (Fig. 11 and Fig. 12). Finally, Fig. 14 illustrates the inverse correspondence between the

447 density and magnetisation contrasts observed in the study area; magnetic susceptibility
448 contours show a good correlation with the negative gravity anomalies, indicating that
449 magnetic bodies are also rocks with densities smaller than the average density of the crust in
450 the region.
451
452 **4.2 Integrated user-driven modelling**
453 The 2.5D user-guided trial-and-error integrated modelling of gravity (Fig. 5) and magnetic
454 (Fig. 7) data was performed along three profiles (Fig. 2, Fig. 5 and Fig. 7). Surface geological
455 information was also incorporated into the process. In particular, the regional shear zones
456 were imposed as limits on the large crustal compartments. The direct modelling approach is
457 based on Talwani et al. (1959), in which the magnetic and gravity anomalies are generated
458 by anomalous bodies represented by closed polygons. For each polygon, the density and
459 susceptibility values are assumed to be constant. A priori geophysical and geological
460 information can be incorporated by specifying the geometry and position of the anomalous
461 bodies, thus reducing the non-uniqueness of the solution. As a result, the integrated
462 modelling technique is inherently richer than the automatic inversion approach described in
463 Section 4.1.
464 Profile 1 (Fig. 2, Fig. 5, Fig. 7 and Fig. 15) is 122 km long and has a NW-SE
465 orientation extending from the west of the Rio Piranhas-Seridó Domain to the Patos shear
466 zone (PSZ). The profile location was chosen to characterise the crustal structure at the
467 connection between **SB** and the Patos shear zone. The intercepted region underwent
468 extensive partial melting of the crust during the Pan-African/Brasiliano orogeny (Corsini et
469 al., 1991; Tommasi et al., 1995; Achanjo et al., 2013). The profile also intersects the Santa
470 Luzia dome (Achanjo et al., 2013), which is the main area of the occurrence of migmatites.

Profile 2 (Fig. 2, Fig. 5, Fig. 7 and Fig. 16) is 103 km long and has a NW-SE orientation, crossing the basement rocks of the Rio Piranhas-Seridó Domain, the Seridó Group metasediments and the central part of **SB** and, finally, it intercepts the Picuí-João Câmara shear zone (PJCSZ). The purpose of this profile was to ascertain the crustal structure of the central part of the study area and to correlate it with the southernmost (profile 1) and northernmost (profile 2) parts (Fig. 2).

Profile 3 (Fig. 2, Fig. 5, Fig. 7 and Fig 17) also has a NW-SE orientation and is 74 km long. This profile was chosen to characterise the crustal architecture at the north end of the study area near to the border of the long-wavelength magnetic anomaly (Fig. 5 and Fig. 6) where this anomaly is attenuated.

*4.2.1 Modelling assumptions*

Geological and geophysical constraints are imposed in the integrated modelling in order to incorporate all available information into the models. The main constraints are described below:

1) Only the induced component of magnetisation is considered because the integrated analysis of magnetic anomalies with geological information has shown that the remnant component of magnetisation is regionally negligible for the study area;

2) The boundaries of the anomalous bodies are admitted to be the surfaces where both density and magnetic susceptibility contrasts occur;

3) The estimates given by Oliveira and Medeiros (2012) for the Moho surfaces along the three profiles (Figs. 15–17) are adopted. These estimates were obtained from the isostatic response of the lithosphere due to topographic loads, where the lithosphere is assumed to be laterally uniform and the compensation surface is the Mohorovicic discontinuity associated with the crust-mantle interface;

4) The estimates given by Lima et al. (2015) for the surface separating the upper and lower crust along three profiles (Figs. 15–17) are adopted. These estimates result from the interpretation of high-quality seismic refraction/wide-angle reflection. Note that the depths to this surface range from 15 km to 18 km (Figs. 15–17), approximately. Because the maximum depth for the magnetic sources is assumed to be 17.5 km (the previously estimated depth at which the Curie temperature is reached), we adopted the depth to the interface between the upper and lower crust isthe maximum depth to the bottom of the anomalous magnetic sources;

5) Density values for the upper crust (2.7 kg/cm$^3$), lower crust (2.9 g/cm$^3$) and mantle (3.3 g/cm$^3$) used by Osako et al. (2011) to model a gravity profile of 750 km along a NW-SE cross-section in the northern part of the **BP** are adopted;

6) Average values of magnetic susceptibility and density for the main lithologies of **SB** are obtained from the measurements of the cores of borehole FD-SE-001 (Fig. 8);

7) The limits of outcropping bodies and position of shear zones are determined from the geological map. On the other hand, dip and depth of the anomalous sources result from the geophysical modelling;

8) Anomalous bodies less than 1.0 km thick are excluded from the models.

The results of the integrated modelling of gravity and magnetic data are below presented. The main modelled anomalous sources are referenced in Figs. 15–17 by the letters A, B, C, and D. Note that in all profiles, each letter represents the same body. In addition, the same letters are used to identify the main magnetic sources in Fig. 9, which results from the automatic inversion of the magnetic data.

*4.2.2 Profile 1*

Most of the observed anomalies are fitted (Fig. 15a-b) by anomalous bodies with positive contrasts of susceptibility and negative contrasts of density relative to the background values

of the upper crust, particularly bodies A, B and C in the central part of the profile (Fig. 15c). Note that the limits of these bodies are shear zones and that the average top depth of the bodies is approximately 5 km. Bodies A, B and C (each with an average width of approximately 16 km), together with body E (Fig. 9 and Fig. 15c), form a 50-km wide regional domed structure.

An increase in the estimated magnetic susceptibilities is observed from the northwest to the southeast along the profile. Body A occurs where the basement rocks of **SB** outcrop. Bodies B and C, located between the Várzea (VSZ in Fig. 15c) and Umburana (USZ in Fig. 15c) shear zones, are located in the central part of **SB**. The influence of bodies with characteristics correlated to the Seridó Group metasediments (e.g. S3 in Fig. 15c) is minor. Such secondary bodies represent restricted and thin metasediment sheets (Fig. 3e-f). These are located between the domical bodies (A, B and C in Fig. 15c) and are close to the shear zones.

In the resulting model, the magnetic bodies making significant contributions to the magnetic anomalies have their greatest expressions at depths greater than 5 km. Thus, the Santa Luzia dome (S2 in Fig. 15c) is part of a secondary dome associated with body C. In other words, the model shows that the Santa Luzia dome is only a small outcropping from a larger crustal domical structure.

*4.2.3 Profile 2*

The model for profile 2 shares similar characteristics as the profile 1 model. In particular, most of the observed anomalies are fitted (Fig. 16a–b) by anomalous bodies with positive contrasts of susceptibility and negative contrasts of density relative to the background values of the upper crust, particularly bodies A, B, C, and D (Fig. 16c). However, for this profile, it becomes clear that the highest values of susceptibility are estimated for the anomalous bodies are located in the central part of **SB** (bodies B and C in Fig. 16c). The positions of

these bodies coincide with a smooth uplift in the interface separating the upper and lower crust. Secondary bodies that might be correlated with **SB** metasediments also appear in the form of synforms (Fig. 15c); however, here they are thicker than for profile 1 and reach depths of up to 3.5 km.

*4.2.4 Profile 3*

The resulting model for profile 3 shares similar characteristics to the models derived from profiles 1 and 2. However, the strength of the observed anomalies and the total width of the modelled bodies suggest attenuation of the domical structure in this region. Note also that the upper crust adjacent to the domical structure (F in Fig. 17c) was modelled with a slightly higher value of susceptibility than in the profile 1 and profile 2 models.

### 4.3 Conceptual model of the domical structure

Although the models shown in Fig. 9 and Figs. 15–17 were independently estimated based on very different assumptions and modelling approaches, they are consistent with each other. In particular, Fig. 15c, Fig. 16c and Fig. 17c show that regardless of the approach, the depths to the tops and the positions of the anomalous sources are in good agreement. In addition, the magnetic susceptibility values estimated using the automatic inversion are of the same order of magnitude as those required to fit the observed anomalies in the integrated models. Moreover, the estimated distribution of susceptibility obtained from the automatic inversion of magnetic data (which has no geological constraints) shows a very good correlation with the boundaries of the modelled magnetic sources based on the integrated modelling, and also with the mapped shear zones (Fig. 9).

A schematic (non-scaled) 3D conceptual model synthesising the two modelling results and their correlations with the available geological information is shown in Fig. 18. In relation to the geological information, we incorporated as much of this as possible (given

the scale of the block diagrams), including information on outcropping lithologies, shear zones, antiforms, synforms, and other structural lineaments. In the three diagrammatic blocks in the model, the main modelled bodies form an arcuate pattern of the regional crustal-scale domical structure.

Note that shear zones serve both as external and internal limits to the domical structure. In addition, note that a good correlation was observed between the outcropping geologic units and their continuity with the subsurface of the modelled bodies. In particular, in the central parts of the crustal sections of block diagrams 1 and 2, the presence of the domical structures was reinforced by mapped antiforms and structural lineaments. Moreover, the metasediments of the Seridó Group are thicker in the central part of **SB** (block diagram 2). Finally, in block diagram 3, in accordance with the derived models, the width of the regional domical structure is smaller, thus showing that the expression of this domical structure is attenuated in a northerly direction.

## 5. DISCUSSION

The expressive regional magnetic anomaly that occurs in the south-central part of **SB** (Fig. 5 and Fig. 6) and the associated gravity anomalies (Fig. 7) are associated with a large volume of rocks with positive susceptibility contrast and negative density contrast. Correlation with surface geology suggests that this anomalous source is composed of magnetite-bearing inhomogeneous migmatites and granites that result from the partial melting of basement rocks and magmatic injections.

Our geophysical model (Fig. 18) presents a crustal domical structure in the south-central part of **SB**. This structure is composed of four main elongated bodies with long axes oriented in the NE-SW direction (changing to E-W near to the Patos shear zone) surrounded by body E. The four elongated bodies are the geophysical expressions of the rock material,

595 resulting from the concentration of partially melted basement rocks and magmatic injections.
596 We stress, however, that the geometry of these bodies (Fig. 9 and Figs. 15–17) is only an
597 approximation of the crustal domical structure. It is probable that each modelled body
598 represents the shell surrounding many other smaller bodies varying in composition and
599 shape, and with varying densities and magnetic susceptibilities.

600 We attribute the formation processes of this crustal domical structure to the tectonic
601 events associated with the Pan-African/Brasiliano orogeny, particularly the ages given by
602 Archanjo et al. (2013) (c. 575 Ma) and Viegas et al. (2014) (c. 566 Ma) for the tectonic
603 regime producing a general extrusion (or tectonic escape) to the northeast of the northern
604 part of the **BP** (Brito Neves et al., 2000; Alkmim et al., 2001; Ganade de Araújo et al., 2014).
605 The formation of the regional gneiss dome in **SB** would, thereby, have been temporally
606 coincident with the collision of the **BP** and the São Francisco-Congo craton during the
607 Ediacaran.

608 The relative vertical positioning (in relation to the metasediments) of the top of the
609 bodies forming the regional crustal domical structure, and the processes related to
610 denudation and weathering in the area, mean that the tops of the bodies outcrop in some
611 locations. This is true in the case of the Santa Luzia dome. That is, the Santa Luzia dome is
612 a local small-scale outcropping dome of the larger regional-scale domical structure. In
613 addition, the metasediments of the Seridó Group occur along synforms surrounding the four
614 internal elongated domical bodies. The limits of the crustal domical structure (both external
615 and internal divisions) are shear zones, in accordance with the strong tectono-structural
616 control they exert in the **BP**.

617 According to the literature, the partial melting of rocks occurred under high-
618 temperature and low-pressure conditions during the **BP** amalgamation and in association
619 with the Neoproterozoic dextral transpressive deformation regime of **SB**. The Acari granitoid

620 and Santa Luzia anatetic dome are examples of the resulting rocks, having formed under
621 high-temperature/low-pressure conditions at approximately 575 Ma (Archanjo et al., 2013).
622 Evidence that the partial melting involved the metasediments of the Seridó Group
623 includes the fact that large amounts of megaxenolites from these supracrustals are found in
624 areas where intense anatexis is identified. For example, over one of the modelled elongated
625 bodies (B in Fig. 9 and Fig. 16), Cabral Neto et al. (2019) recently mapped peraluminous
626 granitoids that occur as a large stock with associated intrusive dikes in the Rio Piranhas-
627 Seridó Domain. In relation to the main stock, these authors report the common occurrence
628 of garnet-biotite schist xenoliths of the Seridó Formation. In addition, they obtained a U-Pb
629 zircon age of 592 ± 2 Ma for the crystallisation of the Jardim do Seridó Suite, which is
630 compatible with the peak of deformation, magmatism and metamorphism (at c. 600 Ma)
631 caused by the Pan-African/Brasiliano orogeny (Brito Neves et al., 2014). Moreover, based
632 on the U-Pb ages of migmatites and granites dated by Archanjo et al. (2008), Archanjo et al.
633 (2013) and Viegas et al. (2014), Cavalcante et al. (2016) inferred that partial melting and
634 magmatism events remained active for at least 25 Ma in the Patos-Seridó system.
635 The existence of a large volume of migmatites in the crust of the Patos-Seridó System
636 has been suggested as evidence of the partial melting of the deeper parts (or roots) of the
637 Pan-African/Brasiliano orogenic belt (Archanjo et al., 2013; Viegas et al., 2014; Cavalcante
638 et al., 2016). Archanjo et al. (2013) suggested that a migmatised zone existed in the
639 southwest region of the Acari granitoid (A in Fig. 2), and that the Santa Luzia anatetic dome
640 was a part of this zone. In addition, Cavalcante et al. (2016) suggested that the Patos shear
641 zone (PSZ) would be a preferential area/channel for the migration of melt derived from the
642 partial melting. These suggestions are reinforced by our proposal of a regional crustal
643 domical structure in **SB**. In particular, the correspondence shown in this work between the
644 long-wavelength magnetic anomaly that occurs in the south-central part of **SB** (Fig. 5 and

645 Fig. 6), and the occurrence of magnetite-bearing migmatites and granites (Archajno et al.,
646 2013; Viegas et al., 2014), are consistent with the suggestions of Archanjo et al. (2013) and
647 Cavalcante et al. (2016).

648 The geophysical model synthesised in Fig. 18 is also consistent with several other
649 types of geological evidence. For example, Caby et al. (1991) pointed out the existence of a
650 general arcuate pattern for the lithology of **SB** near to the Patos shear zone. They reported
651 also that (pre-Pan-African/Brasiliano orogeny) basement rocks appear as elongated domes
652 whilst Proterozoic covers produce synformal structures associated with shear zones. In
653 addition, the shear zones (especially the deepest ones) played a very important role in the
654 segregation, rising and conditioning of the partially melted material (Vanderhaeghe, 2009;
655 Neves et al., 2012; Cavalcante et al., 2016). The correlation between the limits of the gravity
656 (Fig. 7) and magnetic (Fig. 5 and Fig. 6) anomalies with shear zones support this form of
657 structural control.

658 The accumulation of large volumes of melt at mid and deep crustal levels during
659 orogenesis produces extreme changes in the rheological behaviour of the crust (Whitney et
660 al., 2004). Partial melting influences the location of deformation and the general structure of
661 the lithosphere (Cavalcante et al., 2016). In this scenario, shear zones might indicate the
662 limits of deformational corridors (Cunningham, 2010) and accommodate blocks with
663 different rheology (Tommasi et al., 1995). Considering that the forming processes of gneiss
664 domes involve important heat and mass transfer mechanisms (Whitney et al., 2004), these
665 structures can indicate the location of strongly deformed regions and key tectonic boundaries
666 (Cunningham, 2010).

667 In specific reference to the **BP**, Corsini et al. (1991) suggested that deformation
668 would have been transferred from the eastern end of the Patos shear zone to **SB**, resulting in
669 bending, transcurrent failure and stretching parallel to the belt direction. These authors

highlight the rotation of the magnetic and gravity anomalies (from NE-SW to E-W near to the Patos shear zone) as discussed by Moreira et al. (1989) to indicate the mechanical continuity between **SB** and the Patos shear zone. Here, we interpret this rotation as being associated with a crustal domical structure. In addition, the occurrence of migmatites in the Patos shear zone and the central portion of **SB** (Archanjo et al., 2013; Viegas et al., 2014) strengthens the temporal association between migmatisation and the role of the Patos shear zone as a continental transform boundary (Brito Neves et al., 2016).

## 6. CONCLUSION

The magnetic map of the Seridó Belt shows an expressive long-wavelength regional anomaly in the south-central part of the area. This anomaly is sigmoidal in shape with a central axis oriented in the NNE-SSW direction rotating to the W near to the Patos shear zone. Local anomalies with small wavelengths and large amplitudes overlap this regional anomaly. The limits of the magnetic anomalies coincide with regional shear zones, thus revealing that the shear zones exert an important tectono-structural control on their formation. At the Earth surface, the limits of the long-wavelength anomaly are defined by the Umburana, Totoró and Patos shear zones to the east, west and south, respectively.

Comparison with gravity data reveals that both the magnetic and gravity anomalies share a common source, namely rocks that are more magnetic and less dense than the surrounding crust. On the other hand, the regional magnetic anomaly spatially coincides with radiometric patterns associated with high concentrations of radioelements in the south-central part of the Seridó Belt. Finally, correlation with surface geology shows that the geophysical anomalies (magnetic, gravity and radiometric) occur in association with inhomogeneous magnetite-bearing migmatites and granites, which were formed from the fusion of the Seridó Belt basement rocks and magmatic injections during the Neoproterozoic.

The existence of a crustal domical structure in the south-central part of the Seridó Belt has been evidenced using two independent modelling approaches. This crustal structure is composed of four main elongated bodies (within a surrounding body) that have long-axes orientations in the NE-SW direction rotating to E-W near to the Patos shear zone. These anomalous bodies are the geophysical expressions of rock volumes formed from the partial melting of basement rocks and magmatic injections.

The relative vertical positioning of the top of the bodies composing the crustal domical structure, and denudation and weathering in the area, mean that the tops of the bodies outcrop in some locations. This is true in the case of the Santa Luzia dome, which is a local outcropping dome of this regional domical structure. In addition, the metasediments of the Seridó Group occur along synforms surrounding the internal structures that form the regional dome.

The formation of this crustal gneiss dome in the Seridó Belt would have occurred during the Ediacaran, when **BP** and the São Francisco–Congo craton were colliding as part of the Pan-African/Brasiliano orogeny. These events contributed to the agglutination of West Gondwana during the Neoproterozoic. Because of the remarkable role of the Patos shear zone in shaping the crustal domical structure, our results corroborate existing assumptions that the Patos shear zone was a very important tectonic control during the Pan-African/Brasiliano orogeny.

## ACKNOWLEDGMENTS

The employed gravity dataset results from surveys done by the universities of Rio Grande do Norte (UFRN), Pernambuco (UFPE), São Paulo (USP), besides the National Observatory (ON/MCTIC), the Brazilian Institute of Geography and Statistics (IBGE), the Geological Survey of Brazil (SGB/CPRM), and the Brazilian Oil and Gas Agency (ANP). The employed aerogeophysical surveys, besides the petrophysical data obtained from the stratigraphic borehole, are part of the SGB/CPRM database. W.E. Medeiros thanks CNPq for the research fellowship and associated grant (Proc. no. 304743/2018-6).

## DATA AVAILABILITY STATEMENT

The aerogeophysical data used in this research are public and available from the site of CPRM-Serviço Geológico do Brasil. In the address http://www.cprm.gov.br/aero/aero.htm, a catalog of the available surveys is presented and, in the address, http://geosgb.cprm.gov.br/downloads/index.php?dir=Levantamentos_Geofisicos&widget=1, specific data files can be downloaded. Other data is not yet public.

## FIGURE CAPTIONS

Figure 1- Geological context of the study area (red rectangle) in northeastern Brazil. On the left side of (a): tectonic framework of the Borborema Province (**BP**), according to Van Schmus et al. (1995). The **BP** is divided in the Northern, Transversal and Southern subprovinces. On the right side of (a): tectonic context of the **BP** during the agglutination of West Gondwana (at c. 600 Ma). b) Close-up on the red rectangle showing the tectonic compartments of the study area. According to Jardim de Sá (1994), the study area is subdivided into the Rio Piranhas-Seridó (RPSD) and São José do Campestre (SJCD) domains by the Picuí-João Câmara shear zone (PJCSZ). The shear zones (SZ) are identified by: TBSZ-Transbrasiliano, JSZ-Jaguaribe, PSZ-Patos, PESZ-Pernambuco and PJCSZ-Picuí-João Câmara.

Figure 2- Simplified geological map of the Seridó Belt (**SB**) (adapted from Angelim et al., 2004). The rectangle in white line delimits the area which was used for the 3D automatic inversion of the aeromagnetic data, whilst the three straight black lines show the profiles location used to perform the 2.5D user-guided integrated modelling of gravity and magnetic data. The curved thin black lines represent the main shear zones internal to the Rio Piranhas-Seridó Domain. On the other hand, the curved thick black lines represent shear zones that separate different tectonic subprovinces or domains. All shear zones result from surface geological mapping, except for the dashed black line that is the inferred continuation of the Totoró shear zone (TSZ) from the geophysical maps. The shear zones (SZ) are identified by: VSZ-Várzea, USZ-Umburana, FMSZ-Frei Martinho, PSZ-Patos, PJCSZ-Picuí-João Câmara, SMSZ-Santa Mônica, and TSZ-Totoró. S1, S2, and S3 identify the outcrops location referred in Fig. 3.

Figure 3- Photographs of reference outcrops. (a) Banded orthogneiss representing the basement rocks of **SB** (S1 in Figs. 2 and 15). During the Neoproterozoic, these rocks suffered partial melting associated with the Pan-African/Brasiliano orogeny. The resulting melt afforded the formation of migmatites that exhibit xenoliths of the basement rocks (shown in b and c) and of equigranular leucogranites (shown in d). Based on field measurements, we observed that the rocks resulting from partial melting often present high values of magnetic susceptibility, the opposite occurring with the basement rocks. In (d), it is still possible to observe the presence of paleosome (mafic) and neosome (felsic) with indications of disordered flow of melted material. The occurrences described in the photographs (b), (c), and (d) were observed by us in a same outcrop of the Santa Luzia anatetic dome (Archanjo et al., 2013). In (e) quartzites of the Equador Formation are shown dipping 50º/287º Az; kinematic indicators of thrust transport were not identified in this outcrop. In (f), a more regional aspect of the same dip of the quartzites is illustrated. The photographs shown in (a), (b-d), and (e-f) were taken in the three outcrops identified by S1, S2, and S3 in Figs. 2 and 15, respectively. Note that S3is positioned in the west limit of the Santa Luzia dome.

Figure 4- False-color red-green-blue (RGB) ternary composition map of Potassium (K in red), equivalent Thorium (eTh in green), and equivalent Uranium (eU in blue) channels, with transparency over the topography. See the caption of Fig. 2 for a description of the overlapping elements.

Figure 5- Total field magnetic anomaly map, after IGRF (International Geomagnetic Reference Field) removal and upward continuation to 1000 m. See the caption of Fig. 2 for a description of the overlapping elements.

Figure 6- Reduced-to-the-pole magnetic anomaly map obtained from Fig. 5. See the caption of Fig. 2 for a description of the overlapping elements.

Figure 7- Bouguer gravity anomaly map. See the caption of Fig. 2 for a description of the overlapping elements.

Figure 8- Stratigraphic borehole FD-SE-001-SGB/CPRM, whose location is shown in Fig. 2. Vertical profiles showing the intercepted lithologies (on the left), density (at the center, on $g/cm^3$), and magnetic susceptibility (on the right, $10^{-3}$ SI on logarithmic scale). Three measurements of density and magnetic susceptibility were done for each meter of the core. The plotted values are the resulting average values.

Figure 9- 3D automatic inversion of the magnetic anomalies. Resulting map of estimates of magnetic susceptibility. The letters A, B, C, and D identify the four main anomalous bodies, which compose the interpreted crustal domical structure. Caicó, Santa Luzia, and Currais Novos are the main cities of the region. See the caption of Fig. 2 for a description of the other overlapping elements.

Figure 10- 3D automatic inversion of the magnetic anomalies. Anomaly used as observed data in the inversion process (a), modelled anomaly that resulted from the inversion process (b), and fit between the two anomalies along the profiles 1, 2, and 3 shown as white lines in (a) and (b). The magnetic anomaly shown in (a) is obtained from the magnetic anomaly shown in Fig. 5 (area in the white rectangle) by subtracting its average value. Removing this

813 constant from the observed magnetic data (Fig. 5) is a simple way to ensure the condition
814 that magnetic anomalies are dipolar in nature and should present zero mean over the area
815 used in the inversion process.

816

817 Figure 11- 3D automatic inversion of the magnetic anomalies. Overlap of the isovalue
818 contours of the magnetic susceptibility estimates (from Fig. 9) on a simplified version of the
819 geological map. To the east of the Santa Mônica (SMSZ) and Frei Martinho (FMSZ) shear
820 zones, mapped antiforms coincide with the occurrence of high values of magnetic
821 susceptibility. See the caption of Fig. 2 for a description of the overlapping elements.

822

823 Figure 12- 3D automatic inversion of the magnetic anomalies. Overlap of the isovalue
824 contours of the magnetic susceptibility estimates (from Fig. 9) on the false-color RGB
825 ternary radiometric composition map shown in Fig. 4 (K in red, eTh in green and eU in blue).
826 Note that regions showing high values of magnetic susceptibility coincide with radiometric
827 patterns associated with high concentration of the radioelements in the south-central part of
828 the Seridó Belt. See the caption of Fig. 2 for a description of the overlapping elements.

829

830 Figure 13- 3D automatic inversion of the magnetic anomalies. Diagram blocks containing
831 on the Earth surface the RGB ternary radiometric composition shown in Fig. 4 (K in red,
832 eTh in green and eU in blue) and, in the cross-sections (a) to (c), the estimates of magnetic
833 susceptibility shown in Fig. 9. The cross-sections are done along the profiles 3 (a), 2 (b), and
834 1 (c) shown in Figs. 4 and 9. Here the correlation between anomalous magnetic bodies and
835 radiometric patterns associated with high concentration of radioelements (in the south-
836 central part of the Seridó Belt) is well marked.

Figure 14- 3D automatic inversion of the magnetic anomalies. Overlap of the isovalue contours of the magnetic susceptibility estimates (from Fig. 9) on the Bouguer gravity anomaly map (Fig. 7). Note that negative gravity anomalies correlate with regions of high susceptibility values. See the caption of Fig. 2 for a description of the overlapping elements.

Figure 15- Two-and-a-half-dimensional (2.5D) user-guided integrated modelling of magnetic and gravity data. Profile 1. Observed and modelled magnetic anomalies (a), observed and modelled gravity anomalies (b), crustal cross-section showing the modelled bodies. Major contributions to fit the observed fields are given by the anomalous bodies A, B, and C. Note that these bodies are more magnetic and less dense than the surrounding upper crust. The shear zones locations on the Earth surface are given by geological mapping. The shear zones (SZ) are identified by: VSZ-Várzea, USZ-Umburana, PSZ-Patos, and PJCSZ-Picuí-João Câmara. Arrows S1, S2 and S3 indicate the outcrops locations shown in Fig. 3 and whose photographs are given in Fig. 3.

Figure 16- Two-and-a-half-dimensional (2.5D) user-guided integrated modelling of magnetic and gravity data. Profile 2. Observed and modelled magnetic anomalies (a), observed and modelled gravity anomalies (b), crustal cross-section showing the modelled bodies. Major contributions to fit the observed fields are given the anomalous bodies A, B, C, and D. Note that these bodies are more magnetic and less dense than the surrounding upper crust. The shear zones locations on the Earth surface are given by geological mapping. The shear zones (SZ) are identified by: VSZ-Várzea, USZ-Umburana, FMSZ- Frei Martinho and PJCSZ-Picuí-João Câmara.

Figure 17- Two-and-a-half-dimensional (2.5D) user-guided integrated modelling of magnetic and gravity data. Profile 3. Observed and modelled magnetic anomalies (a), observed and modelled gravity anomalies (b), crustal cross-section showing the modelled bodies. Major contributions to fit the observed fields are given by the anomalous bodies B and D. Note that these bodies are more magnetic and less dense than the surround upper crust. The shear zones locations on the Earth surface are given by the surface geology. The shear zones (SZ) are identified by: TSZ-Totoró, USZ-Umburana, FMSZ-Frei Martinho, SMSZ-Santa Mônica, and PJCSZ-Picuí-João Câmara.

Figure 18- Conceptual model of the crustal domical structure in the Seridó Belt region. The conceptual model is shown as schematic diagram blocks (non-scaled) for the crust along the profiles 1, 2 and 3 used in the integrated magnetic and gravity modelling (Figs 15-17). Note that shear zones serve both as external and internal limits to the domical structure. Drawn litology, antiforms, synforms, and other structural lineaments follow, as much of this as possible, the available geological information on the Earth surface.

885 **REFERENCES**

886 Alkmim, F.F., Marshak, S., Fonseca, M.A., 2001. Assembling West Gondwana in the
887 Neoproterozoic: clues from the São Francisco craton region, Brazil. Geology 29, 319–
888 322. https://doi.org/10.1130/0091-7613(2001)029<0319:AWGITN>2.0.CO;2.

889 Almeida, F.F.M., Hasui, Y., Brito Neves, B.B., Fuck, R.A., 1981. Brazilian structural
890 provinces: an introduction. Earth-Sci. Rev. 17 (1-2), 1-29. https://doi.org/10.1016/0012-
891 8252(81)90003-9.

892 Angelim, L.A.A., Vasconcelos, A.M., Gomes, J.R.C., Wanderley, A.A., Forgiarini, L.L.,
893 Medeiros, M. de F., 2004. Folha SB.24-Jaguaribe. In: Schobbenhaus, C., Gonçalves,
894 J.H., Santos, J.O.S., Abram, M.B., Leão Neto, R., Matos, G.M.M., Vidotti, R.M.,
895 Ramos, M.A.B., Jesus, J.D.A. de (Eds.). Carta Geológica do Brasil ao Milionésimo.
896 Sistema de Informações Geográficas - SIG, Programa Geologia do Brasil. CPRM,
897 Brasília, CD-ROM. http://www.cprm.gov.br/publique/Geologia/Geologia-
898 Basica/Carta-Geologica-do-Brasil-ao-Milionesimo-298.html (accessed 21 October
899 2019).

900 Archanjo, C.J., Hollanda, M.H.B.M., Rodrigues, S.W.O., Brito Neves, B.B., Armstong, R.,
901 2008. Fabrics of pre- and syntectonic granite plutons and chronology of shear zones in
902 the Eastern Borborema Province, NE Brazil. J. Struct. Geol. 30 (3), 310-336.
903 https://doi.org/10.1016/j.jsg.2007.11.011.

904 Archanjo, C.J., Viegas, L.G., Hollanda, M.H.B.M., Souza, L.C., Liu, D., 2013. Timing of
905 the HT/LP transpression in the Neoproterozoic Seridó Belt (Borborema Province,
906 Brazil): Constraints from U-Pb (SHRIMP) geochronology and implications for the
907 connections between NE Brazil and West Africa. Gondwana Res. 23 (2), 701-714.
908 https://doi.org/10.1016/j.gr.2012.05.005.

909 Ayarza, P., Martínez Catalán, J.R., 2007. Potential field constraints on the deep structure of
910 the Lugo gneiss dome (NW Spain). Tectonophysics. 439 (1-4), 67-87.
911 https://doi.org/10.1016/j.tecto.2007.03.007.
912 Baldim, M.R., Oliveira, E.P., 2016. Anatomy of the Alto Alegre gneiss dome, São Francisco
913 Craton, Brazil: A geological record of transpression along a Paleoproterozoic arc-
914 continent collision zone. Precambrian Res. 286, 250-268.
915 https://doi.org/10.1016/j.precamres.2016.10.004.
916 Blakely, R.J., 1995. Potential Theory in Gravity and Magnetic Applications. Cambridge:
917 Cambridge University Press. 441pp. https://doi.org/10.1017/CBO9780511549816.
918 Brito Neves, B.B., Cordani, U.G., 1991. Tectonic evolution of South America during the
919 Late Proterozoic. Precambrian Res. 53 (1-2), 23-40. https://doi.org/10.1016/0301-
920 9268(91)90004-T.
921 Brito Neves, B.B., Santos, E.J., Van Schmus, W.R., 2000. Tectonic history of the Borborema
922 Province, NW Brazil. In: Cordani, U.G., Milani, E.J., Thomaz-Filho, A., Campos, D.A.
923 (Eds.), Tectonic Evolution of South America. 31st International Geological Congress,
924 Rio de Janeiro, pp. 151–182.
925 Brito Neves, B.B., Fuck, R.A., Pimentel, M.M., 2014. The Brasiliano collage in South
926 America: a review. Braz. J. Geol. 44 (3), 493–518. http://dx.doi.org/10.5327/Z2317-
927 4889201400030010.
928 Brito Neves B.B., Santos E.J., Fuck R.A., Santos L.C.M.L., 2016. A preserved early
929 Ediacaran magmatic arc at the northernmost portion of the Transversal Zone central
930 subprovince of the Borborema Province, Northeastern South America. Brazilian Journal
931 of Geology, 46, 491-508. http://dx.doi.org/10.1590/2317-4889201620160004.
932 Brown, R.L., Journeay, J.M., Lane, L.S., Murphy, D.C., Rees, C.J., 1986. Obduction,
933 backfolding and piggyback thrusting in the metamorphic hinterland of the southeastern

934 Canadian Cordillera. J. Struct. Geol. 8 (3-4), 225-268. https://doi.org/10.1016/0191-
935 8141(86)90047-7.
936 Brun, J.P., 1983. L'origine des domes gneissiques: Modeleset tests. Bull. Soc. Geol. Fr. 25,
937 219-228. https://doi.org/10.2113/gssgfbull.S7-XXV.2.219.
938 Cabral Neto, I., de Medeiros, V., Cavalcante, R., Fernandes, P., Silveira, F., Dantas, E.,
939 Rodrigues, J., Cunha, I., Paes, V., Santos, L., Pinho, I., 2019. Jardim do Seridó Suite:
940 first example of Ediacaran peraluminous magmatism in the Rio Piranhas-Seridó
941 Domain, Borborema Province, Northeast Brazil. J. Geol. Surv. Braz. 2 (2), 119-136.
942 https://doi.org/10.29396/jgsb.2019.v2.n2.3.
943 Caby, R., Arthaud, M.H., 1986. Major Precambrian nappes of the Brazilian belts, Ceará,
944 Northeast Brazil. Geology. 14 (10), 871–874. https://doi.org/10.1130/0091-
945 7613(1986)14<871:MPNOTB>2.0.CO;2.
946 Caby, R., Sial, A.N., Arthaud, M.H., Vauchez, A., 1991. Crustal evolution and the Brasiliano
947 orogeny in northeast Brazil. In: Dallmeyer, R.D., Lé corché, J.P. (Eds.), The West
948 African Orogens and Circum-Pacific-Atlantic Correlatives. Springer, Berlin,
949 Heidelberg, pp. 373–397. https://doi.org/10.1007/978-3-642-84153-8_16.
950 Cavalcante, G.C.G., Viegas, G., Archanjo, C.J., Silva, M. E., 2016. The influence of partial
951 melting and melt migration on the rheology of the continental crust. J. Geodyn. 101,
952 186-199. https://doi.org/10.1016/j.jog.2016.06.002.
953 Caxito, F.A., Uhlein, A., Dantas, E.L., Stevenson, R., Salgado, S.S., Dussin, A.I., Sial, A.N.,
954 2016. A complete Wilson Cycle recorded within the Riacho do Pontal Orogen, NE
955 Brazil: implications for the Neoproterozoic evolution of the Borborema Province at the
956 heart of West Gondwana. Precambrian Res. 282, 97-120.
957 https://doi.org/10.1016/j.precamres.2016.07.001.

958 Constable, S.C., Parker, R.L., Constable, C.G., 1987. Occam's inversion: A practical
959 algorithm for generating smooth models from electromagnetic sounding data.
960 Geophysics. 52 (3), 289-300. http://dx.doi.org/10.1190/1.1442303.
961 Corsini, M., Vauchez, A., Archanjo, C.J., Jardim de Sá, E.F., 1991. Strain transfer at a
962 continental scale from a transcurrent shear zone to a transpressional fold belt: the Patos-
963 Seridó belt system, north-eastern Brazil. Geology. 19 (6), 586-589.
964 https://doi.org/10.1130/0091-7613(1991)019%3C0586:STACSF%3E2.3.CO;2.
965 Corsini, M., Lambert De Figueiredo, L., Caby, R., Féraud, G., Ruffet, G., Vauches, A., 1998.
966 Thermal history of the Pan/African – Brasiliano Borborema province of the northeast
967 Brazil, deduced from 40AR/39AR analysis. Tectonophysics. 285 (1-2), 103-117.
968 https://doi.org/10.1016/S0040-1951(97)00192-3.
969 Crowley, J.L., Brown, R.L., Parrish, R.R., 2001. Diachronous deformation and a strain
970 gradient beneath the Selkirk allochthon, northern Monashee complex, southeastern
971 Canadian Cordillera. J. Struct. Geol. 23 (6-7), 1103-1121.
972 https://doi.org/10.1016/S0191-8141(00)00179-6.
973 Cunningham, D., 2010. Tectonic setting and structural evolution of the late Cenozoic Gobi
974 Altai orogen. In: Kusky, T.M., Zhai, M.G., Xiao, W.J. (Eds.), The Evolving Continents:
975 Understanding Processes of Continental Growth and Stabilization, Geol. Soc. Lond.
976 Spec. Publ. 338 (1), pp. 361-387. http://dx.doi.org/10.1144/SP338.17.
977 Cutts, K., Lana, C., Alkmim, F., Farina, F., Moreira, H., Coelho, V., 2019. Metamorphism
978 and exhumation of basement gneiss domes in the Quadrilátero Ferrífero: Two stage
979 dome-and-keel evolution? Geosci. Front. 10 (5), 1765-1787.
980 https://doi.org/10.1016/j.gsf.2019.02.009.

981 Dantas, E.L., 1992. Evolução tectono-magmática do maciço polidiapírico São Vicente-
982 Florânia – RN. M.Sc. Thesis. Universidade Estadual Paulista, Instituto de Geociências
983 e Ciências Exatas, pp. 272.
984 Dantas, E.L., 1997. Geocronologia U-Pb e Sm-Nd de terrenos arqueanos e
985 paleoproterozóicos do Maciço Caldas Brandão, NE do Brasil. Ph. D. Thesis.
986 Universidade Estadual Paulista, Instituto de Geociências e Ciências Exatas, pp. 206.
987 D'el-Rey Silva, L.J.H., 1995. The evolution of basement gneiss domes of the Sergipano fold
988 belt (NE Brazil) and its importance for the analysis of Proterozoic basins. J. S. Am.
989 Earth Sci. 8 (3-4). 325-340. https://doi.org/10.1016/0895-9811(95)00017-A.
990 Dixon, J.M., 1987. Mantled gneiss domes. In: Structural Geology and Tectonics.
991 Encyclopedia of Earth Science. Springer, Berlim, Heidelberg.
992 Ellis, R.G., Wet, B., Macleod, I.N., 2012. Inversion of magnetic data from remanent and
993 induced sources. In: 22nd Annual Australian Society of Exploration Geophysicists
994 Conference and Exhibition, Brisbane, Electronic Abstracts, 1-4.
995 https://doi.org/10.1071/ASEG2012ab117.
996 Eskola, P.E., 1949. The problem of mantled gneiss domes. Quart. J. Geol. Soc. London. 104,
997 461-476. https://doi.org/10.1144/GSL.JGS.1948.104.01-04.21.
998 Fletcher, R.C., 1972. Application of a mathematical model to the emplacement of mantled
999 gneiss domes. Am. J. Sci. 272 (3), 197–216. https://doi.org/10.2475/ajs.272.3.197.
1000 Ganade de Araújo, C.E., Weinberg, R.F., Cordani, U.G., 2014. Extruding the Borborema
1001 Province (NE-Brazil): a two-stage Neoproterozoic collision process. Terra Nova. 26, 1–
1002 12. https://doi.org/10.1111/ter.12084.
1003 Grujic, D., 2006. Channel flow and continental collision tectonics: An overview. In: Law,
1004 R.D., Searle, M.P., Godin, L. (Eds.), Channel Flow, Ductile Extrusion and Exhumation

in Continental Collision Zones, Geol. Soc. Lond. Spec. Publ. 268, pp. 25-75. http://dx.doi.org/10.1144/GSL.SP.2006.268.01.02.

Hollanda, M.H.B.M., Archanjo, C.J., Bautista, J.R., Souza, L.C., 2015. Detrital zircon ages and Nd isotope compositions of the Seridó and Lavras da Mangabeira basins (Borborema Province, NE Brazil): evidence for exhumation and recycling associated with a major shift in sedimentary provenance. Precambr. Res. 258, 181–207. https://doi.org/10.1016/j.precamres.2014.12.009.

Jamieson, R.A., Beaumont, C., Nguyen, M.H., Grujic, D., 2006. Provenance of the Greater Himalayan Sequence and associated rocks: predictions of channel flow models. In: Law, R.D., Searle, M.P., Godin, L. (Eds.), Channel Flow, Ductile Extrusion and Exhumation in Continental Collision Zones, Geol. Soc. Lond. Spec. Publ. 268, pp. 165-182. http://dx.doi.org/10.1144/GSL.SP.2006.268.01.07.

Jamieson, R.A., Unsworth, M.J., Harris, N.B.W., Rosenberg, C.L., Schulmann, K., 2011. Crustal melting and the flow of mountains. Elements. 7 (4), 253-260. https://doi.org/10.2113/gselements.7.4.253.

Jardim de Sá, E.F., 1994. A faixa Seridó (província Borborema, NE do Brasil) e seu significado geodinâmico na cadeia brasiliana/pan-africana. Ph.D. Thesis. Universidade de Brasília, Instituto de Geociências, Brasília, pp. 804.

Kodama, K.P., Chapin, D.A., 1984. A detailed gravity study of the Chattolanee Beltimore Gneiss Dome, Maryland, U.S.A. Earth Planet. Sci. Lett. 68 (2), 286-296. https://doi.org/10.1016/0012-821X(84)90160-2.

Kruckenberg, S.C., Vanderhaeghe, O., Ferré, E.C., Teyssier, C., Whitney, D.L., 2011. Flow of partially molten crust and the internal dynamics of a migmatite dome. Naxos, Greece. Tectonics. 30 (3), TC3001. https://doi.org/10.1029/2010TC002751.

1029 Li, Z.X., Bogdanova, S.V., Collins, A.S., Davidson, A., De Waele, B., Ernst, R.E.,
1030 Fitzsimons, I.C.W., Fuck, R.A., Gladkochub, D.P., Jacobs, J., Karlstrom, K.E., Lu, S.,
1031 Natapov, L.M., Pease, V., Pisarevsky, S.A., Thrane, K., Vernikovsky, V., 2008.
1032 Assembly, configuration, and break-up history of Rodinia: a synthesis. Precambr. Res.
1033 160, 171–210. https://doi.org/10.1016/j.precamres.2007.04.021.
1034 Lima, E.S., 1987. Evolução termo-barométrica das rochas metapelíticas da região do Seridó,
1035 Nordeste Brasileiro. Rev. Bras. Geoc. 17 (3), 315–323. https://doi.org/10.25249/0375-
1036 7536.1987315323.
1037 Lima, M.V.A.G., Berrocal, J., Soares, E.P., Fuck, R.A., 2015. Deep seismic refraction
1038 experiment in northeast Brazil: new constraints for Borborema province evolution. J. S.
1039 Am. Earth Sci. 58, 335-349. https://doi.org/10.1016/j.jsames.2014.10.007.
1040 Luz, R.M.N., Julià, J., Do Nascimento, A.F., 2015. Crustal structure of the eastern
1041 Borborema Province, NE Brazil, from the joint inversion of receiver functions and
1042 surface wave dispersion: Implications for plateau uplift, J. Geophys. Res. Solid Earth,
1043 120, 3848-3869. https://doi.org/10.1002/2015JB011872.
1044 MacLeod, I.N., Ellis, R.G., 2013. Magnetic Vector Inversion, a simple approach to the
1045 challenge of varying direction of rock magnetization. In: ASEG Forum on the
1046 Application of Remanent Magnetization. ASEG, 1-4, Melbourne, Australia.
1047 MacLeod, I.N., Ellis, R.., 2016. Quantitative magnetization vector inversion. In: 25th
1048 Geophysical Conference & Exhibition. ASEG-PESA-AIG,1-5, Adelaide, Australia.
1049 Magini, C., Hackspacher, P.C., Legrand, J.M., Neves, B.B.B., Petta, R.A., Sial,
1050 A.N., Dantas, E.L., 1997. Proterozoic tectono-metamorphic evolution of the
1051 SãoVicente-Caicó batolith (State of Rio Grande do Norte). Rev. Bras.
1052 Geociências 16, 257-277.

1053 Martínez Catalán, J.R., Ayarza, P., Álvarez Lobato, F., Villalaín, J.J., Durán Oreja, M.,
1054 Martín Paramio, M., Rodríguez Gómez, S., 2018. Magnetic anomalies in extensional
1055 detachments: The Xistral Tectonic Window of the Lugo Dome (NW Spain). Tectonics.
1056 37 (11), 4261–4284. https://doi.org/10.1029/2017TC004887.
1057 Medeiros, V.C., Cavalcante, R., Cunha, A.L.C., Dantas, A.R., Costa, A.P., Brito, A.A.,
1058 Rodrigues, J.B., Silva, M.A., 2017. O furo estratigráfico de Riacho Fechado (Currais
1059 Novos/RN), Domínio Rio Piranhas-Seridó (Província Borborema, NE do Brasil):
1060 Procedimentos e resultados. Estudos Geológicos (UFPE), 27 (3), 3-44.
1061 Minty, B.R.S., 1997. The fundamentals of airborne gammaray spectrometry. J. Aust. Geol.
1062 Geophys. 17 (2), 39-50.
1063 Moreira, J.A.M., Medeiros, W.E., Lins, F.A.P.L., Archanjo, C.J., 1989. Uma anomalia
1064 magnética de caráter regional no Seridó (RN-PB) e uma discussão de sua origem. In: I
1065 Congr. Bras. SBGf, 592-597, Rio de Janeiro-RJ.
1066 Neves, S.P., Vauchez, A., Feraud, G., 2000. Tectono-thermal evolution, magma
1067 emplacement, and shear zone development in the Caruaru area (Borborema Province,
1068 NE Brazil). Precambrian Res. 99 (1-2), 1–32. https://doi.org/10.1016/S0301-
1069 9268(99)00026-1.
1070 Neves, S.P., Monié, P., Bruguier, O., Rangel da Silva, J.M., 2012. Geochronological,
1071 thermochronological and thermobarometric constraints on deformation, magmatism and
1072 thermal regimes in eastern Borborema Province (NE Brazil). J. S. Am. Earth Sci. 38,
1073 129-146. https://doi.org/10.1016/j.jsames.2012.06.003.
1074 Oliveira, E.P., McNaughton N.J., Windley, B.F., Carvalho, M.J., Nascimento, R.S., 2015.
1075 Detrital zircon U-Pb geochronology and whole-rock Nd-isotope constraints on sediment
1076 provenance in the Neoproterozoic Sergipano orogen, Brazil: From early passive margins

to late foreland basins. Tectonophysics. 662, 183-194. https://doi.org/10.1016/j.tecto.2015.02.017.

Oliveira, R.G., Medeiros, W.E., 2012. Evidences of buried loads in the base of the crust of Borborema Plateau (NE Brazil) from Bouguer admittance estimates. J. S. Am. Earth Sci. 37, 60–76. https://doi.org/10.1016/j.jsames.2012.02.004.

Oliveira, R.G., Medeiros, W.E., 2018. Deep crustal framework of the Borborema Province, NE Brazil, derived from gravity and magnetic data. Precambrian Res. 315, 45-65. https://doi.org/10.1016/j.precamres.2018.07.004.

Osako, L.S., Castro, D.L. de, Fuck, R.A., Castro, N.A., Pitombeira, J.P.A., 2011. Contribuição de uma seção gravimétrica transversal ao estudo da estruturação litosférica na porção setentrional da Província Borborema, NE do Brasil. Rev. Bras. Geof. 29 (2), 309-329. http://dx.doi.org/10.1590/S0102-261X2011000200008.

Rizzotto, G.J., Alves, C.L., Rios, F.S., Barros, M.A.S., 2019. The Nova Monte Verde metamorphic core complex: Tectonic implications for the southern Amazonian craton. J. S. Am. Earth Sci. 91, 154-172. https://doi.org/10.1016/j.jsames.2019.01.003.

Searle, M.P., Treloar, P.J., 2019. Himalayan Tectonics: A Modern Synthesis. Geol. Soc. Lond. Spec. Publ. 483, 1–17. https://doi.org/10.1144/SP483-2019-20.

Sial, A.N. 1986. Granite types in Northeastern Brazil. Current knowledge. Rev. Bras. Geoc. 16 (1), 54-72. https://doi.org/10.25249/0375-7536.19865472.

Soula, J.C., 1982. Characteristics and mode of emplacement of gneiss domes and plutonic domes in central-eastern Pyrenees. J. Struct. Geol. 4 (3), 313-342. https://doi.org/10.1016/0191-8141(82)90017-7.

Soula, J.C., Debat, P., Brusset, S., Bessier, G., Christophoul, F., Deramond, J., 2001. Thrust-related, diapiric, and extensional doming in a frontal orogenic wedge: Example of the

1101 Montagne Noire, Southern French Hercynian Belt. J. Struct. Geol. 23 (11), 1677-1699.
1102 https://doi.org/10.1016/S0191-8141(01)00021-9.
1103 Souza, Z.S., Kalsbeek, F., Deng, X.D., Frei, R., Kokfelt, T.F., Dantas, E.L., Li, J.W.,
1104 Pimentel, M.M., Galindo, A.C., 2016. Generation of continental crust in the northern
1105 part of the Borborema Province, northeastern Brazil, from Archaean to Neoproterozoic.
1106 J. South Am. Earth Sci. 68, 68–96. https://doi.org/10.1016/j.jsames.2015.10.006.
1107 Spector, A., Grant, F.S., 1970. Statistical models for interpreting aeromagnetic data.
1108 Geophysics. 35 (2), 293-302. https://doi.org/10.1190/1.1440092.
1109 Silva, J.B.C., Barbosa, V.C.F., Medeiros, W.E., 2002, Practical applications of uniqueness
1110 theorems in Gravimetry. Part II - Pragmatic incorporation of concrete geologic
1111 information: Geophysics, 67: 795 – 800. https://doi.org/10.1190/1.1484523.
1112 Talbot, C.J., 1974. Fold nappes as asymmetric mantled gneiss domes and ensialic orogeny.
1113 Tectonophysics. 24 (3), 259-276. https://doi.org/10.1016/0040-1951(74)90011-0.
1114 Talwani, M., Worzel, J.L., Landisman, M., 1959. Rapid gravity computations for two-
1115 dimensional bodies with application to the Mendoncino submarine fracture zone. J.
1116 Geophys. Res. 64 (1), 49-59. https://doi.org/10.1029/JZ064i001p00049.
1117 Teyssier, C., Whitney, D., 2002. Gneiss domes and orogeny. Geology. 30 (12), 1139-1142.
1118 https://doi.org/10.1130/0091-7613(2002)030%3C1139:GDAO%3E2.0.CO;2.
1119 Tohver, E., D'Agrella-Filho, M.S., Trindade, R.I.F., 2006. Paleomagnetic record of Africa
1120 and South America for the 1200–500 Ma interval, and evaluation of Rodinia and
1121 Gondwana assemblies. Precambr. Res. 147, 199–222.
1122 Tommasi, A., Vauchez, A., Daudré, B., 1995. Initiation and propagation of shear zones in a
1123 heterogeneous continental lithosphere. J. Geophys. Res. 100 (B11), 22083-22101.
1124 https://doi.org/10.1029/95JB02042.

1125 Trompette, R., 1994. In: Geology of Western Gondwana (2000–500 Ma): Pan-African-
1126 Brasiliano Aggregation of South America and Africa. A.A Balkema, Rotterdam,
1127 Brookfield, pp. 350.
1128 Trompette, R., 1997. Neoproterozoic (~600 Ma) aggregation of Western Gondwana: a
1129 tentative scenario. Precambrian Res. 82 (1-2), 101-112. https://doi.org/10.1016/S0301-
1130 9268(96)00045-9.
1131 Van Schmus, W.R., Brito Neves, B.B., Hackspacher, P.C., Babinski, M., 1995. U/Pb and
1132 Sm/Nd geochronologic studies of the eastern Borborema Province, Northeast Brazil:
1133 initial conclusions. J. S. Am. Earth Sci. 8 (3-4), 267–288. https://doi.org/10.1016/0895-
1134 9811(95)00013-6.
1135 Van Schmus, W.R., Brito Neves, B.B., Williams, I.S., Hackspacher, P.C., Fetter, A.H.,
1136 Dantas, E.L., Babinski, M., 2003. The Seridó Group of NE Brazil, a late Neoproterozoic
1137 pre- to syn-collisional basin in West Gondwana: insights from SHRIMP U-Pb detrital
1138 zircon ages and Sm-Nd crustal residence (TDM) ages. Precambrian Res. 127 (4), 281–
1139 327. https://doi.org/10.1016/S0301-9268(03)00197-9.
1140 Vanderhaeghe, O., Teyssier, C., Wysoczanski, R., 1999. Structural and geochronological
1141 constraints on the role of partial melting during the formation of the Shuswap
1142 metamorphic core complex at the latitude of the Thor-Odin dome, British Columbia.
1143 Can. J. Earth Sci. 36 (6), 917-943. https://doi.org/10.1139/e99-023.
1144 Vanderhaeghe, O., 2009. Migmatites, granites and orogeny: Flow modes of partially-molten
1145 rocks and magmas associated with melt/solid segregation in orogenic belts.
1146 Tectonophysics. 477 (3-4), 119-134. https://doi.org/10.1016/j.tecto.2009.06.021.
1147 Vauchez, A., Neves, S.P., Caby, M., Corsini, M., Egydio Silva, M., Arthaud, M.H., Amaro,
1148 V., 1995. The Borborema shear zone system, NE Brazil. J. S. Am. Earth Sci. 8 (3-4),
1149 247–266. https://doi.org/10.1016/0895-9811(95)00012-5.

1150 Viegas, L.G.F., Archanjo, C.J., Hollanda, M.H.B.M., Vauchez, A., 2014. Microfabrics and
1151 zircon U–Pb (SHRIMP) chronology of mylonites from the Patos shear zone (Borborema
1152 Province, NE Brazil). Precambrian Res. 243, 1-17.
1153 https://doi.org/10.1016/j.precamres.2013.12.020.
1154 Whitney, D.L., Teyssier, C., Vanderhaeghe, O., 2004. Gneiss domes and crustal flow. In:
1155 Whitney, D.L., Teyssier, C., Siddoway, C.S. (Eds.), Gneiss Domes in Orogeny. Geol.
1156 Soc. Am. Spec. Paper. vol. 380, pp. 15-33. https://doi.org/10.1130/0-8137-2380-9.15.
1157 Yin, A., 2004. Gneiss domes and gneiss dome systems. In: Whitney, D.L., Teyssier, C.,
1158 Siddoway, C.S. (Eds.), Gneiss Domes in Orogeny. Geol. Soc. Am. Spec. Paper. vol.
1159 380, pp. 1-14. https://doi.org/10.1130/0-8137-2380-9.15.
1160 Zhang, B., Chai, Z., Yin, C.Y., Huang, W.T., Wang, Y., Zhang, J.J., Wang, X.X., Cao, K.,
1161 2017. Intra-continental transpression and gneiss doming in an obliquely convergent
1162 regime in SE Asia. J. Struct. Geol. 97, 48-70. https://doi.org/10.1016/j.jsg.2017.02.010.
1163 Zietz, I., Haworth, R.T., Williams, H., Daniela, D.L., 1980. Magnetic anomaly map of the
1164 Appalachian orogen. Memorial University of Newfoundland, Map No. 2a, scale
1165 1:2,000,000.
1166

1167

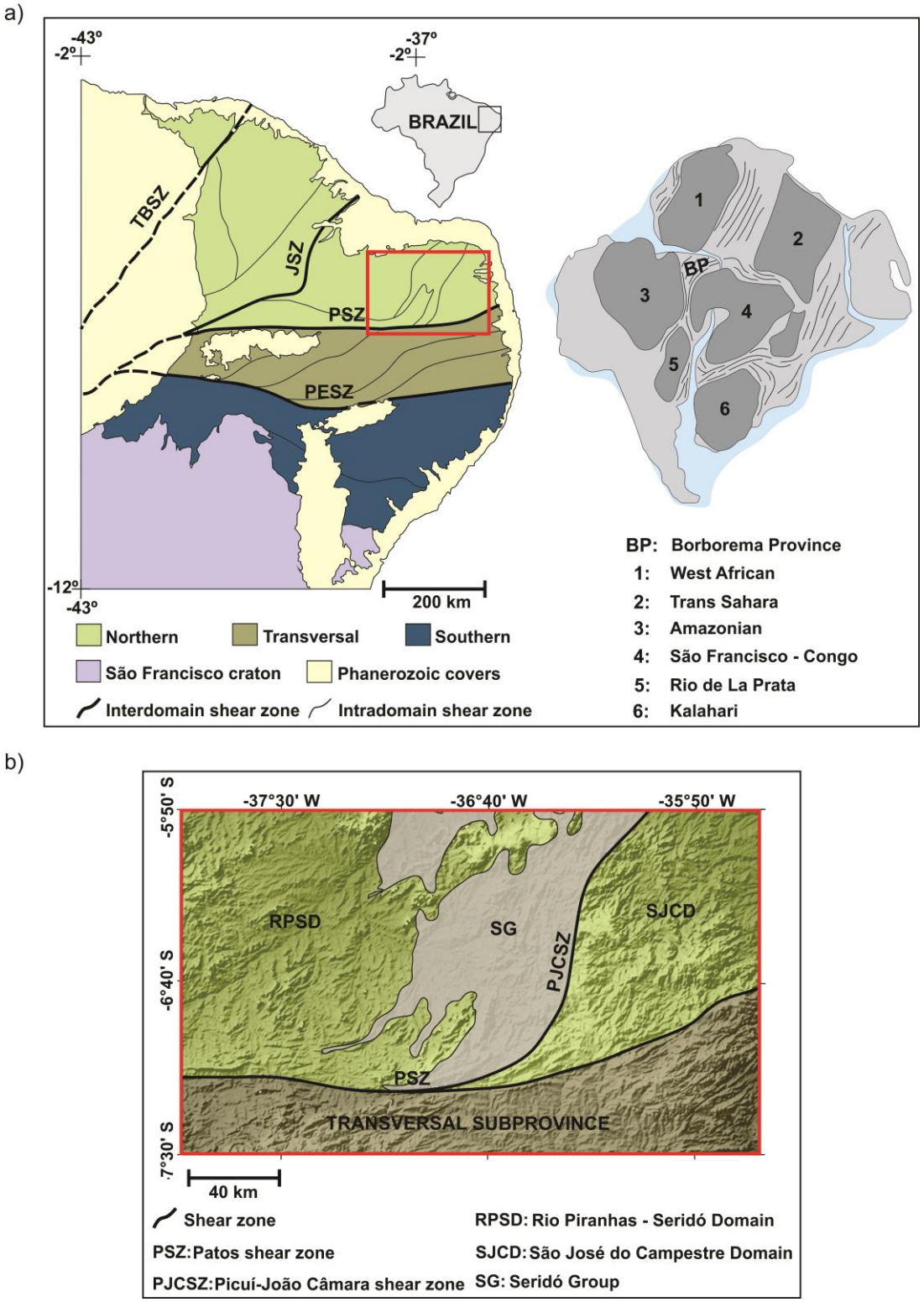


1168

1169

1170 **Figure 1**

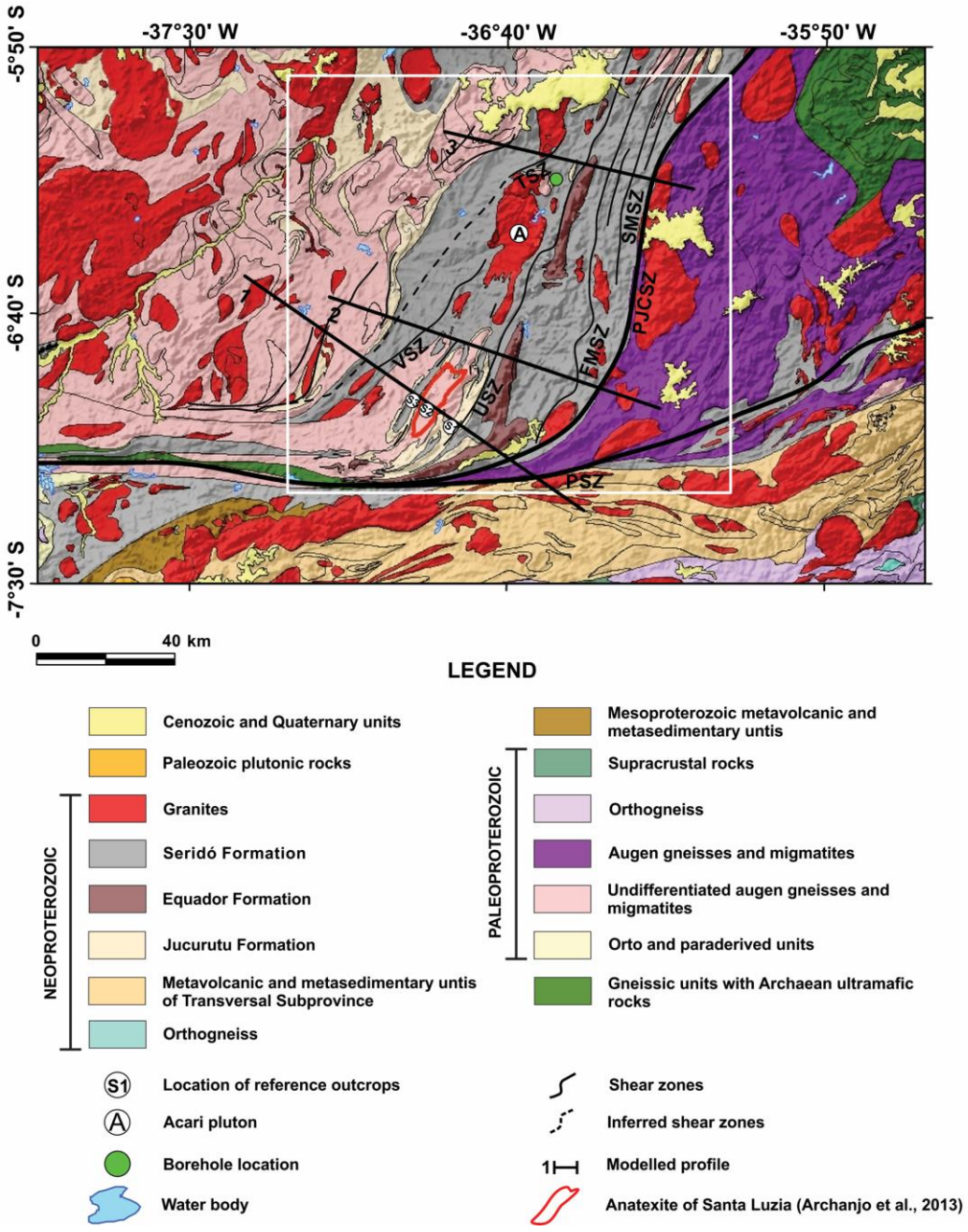
-37°30' W
-36°40' W
-35°50' W
-5°50' S
-6°40' S
-7°30' S
TSZ
SMSZ
PJCSZ
EMSZ
VSZ
USZ
PSZ
A
0
40 km
LEGEND
Cenozoic and Quaternary units
Paleozoic plutonic rocks
Granites
Seridó Formation
Equador Formation
Jucurutu Formation
Metavolcanic and metasedimentary untis of Transversal Subprovince
Orthogneiss
NEOPROTEROZOIC
Mesoproterozoic metavolcanic and metasedimentary untis
Supracrustal rocks
Orthogneiss
Augen gneisses and migmatites
Undifferentiated augen gneisses and migmatites
Orto and paraderived units
Gneissic units with Archaean ultramafic rocks
PALEOPROTEROZOIC
S1
Location of reference outcrops
Acari pluton
Borehole location
Water body
Shear zones
Inferred shear zones
Modelled profile
Anatexite of Santa Luzia (Archanjo et al., 2013)

**Figure 2**

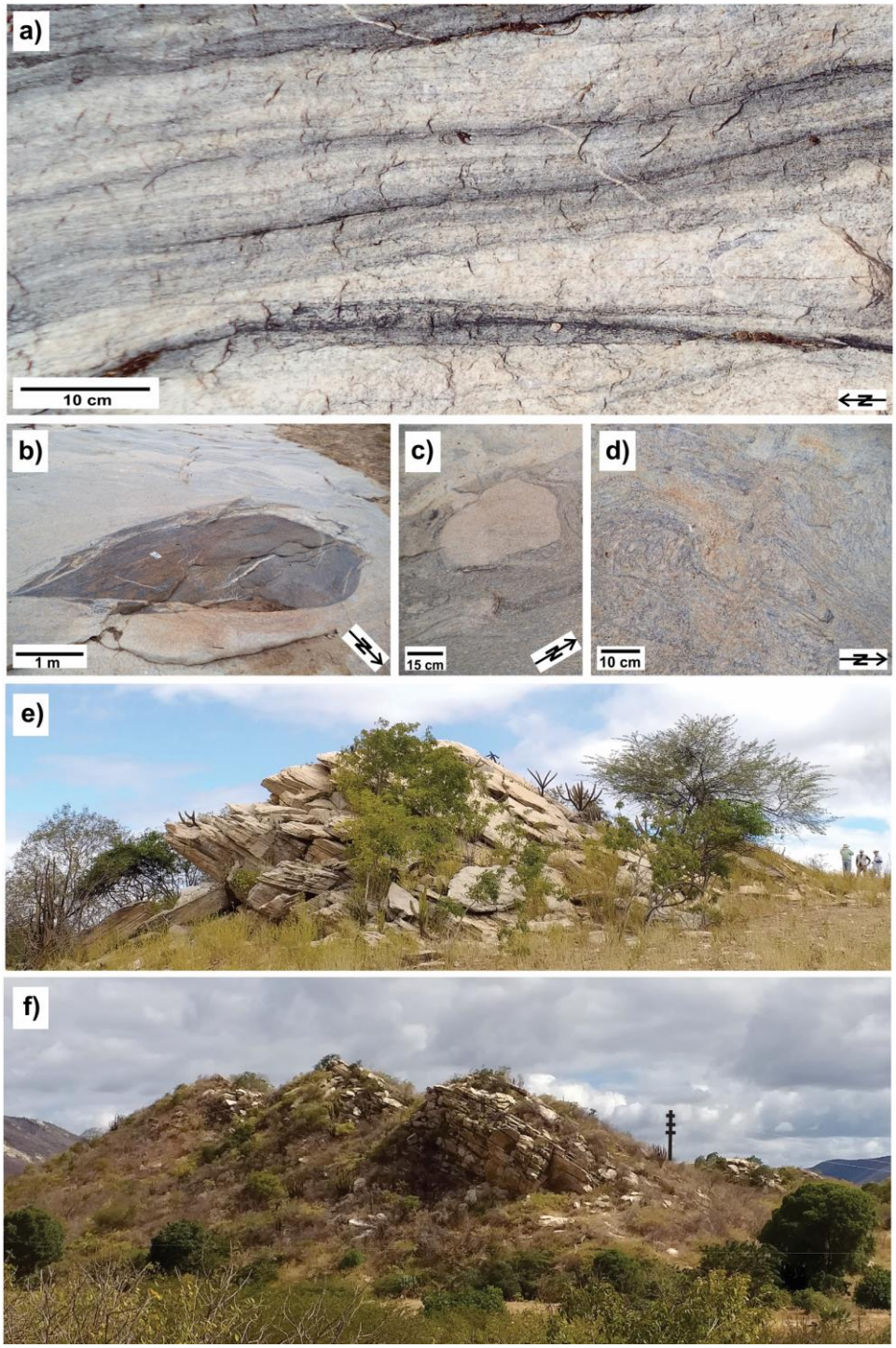


1175

1176

1177 **Figure 3**

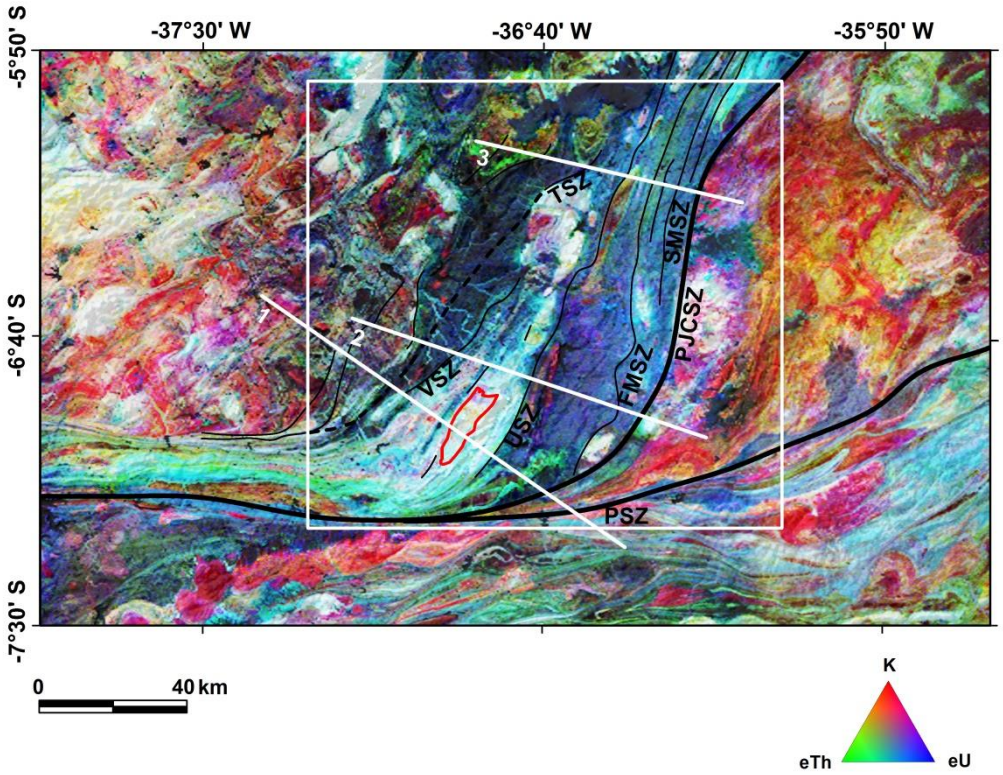


1178

1179

1180 **Figure 4**

1181

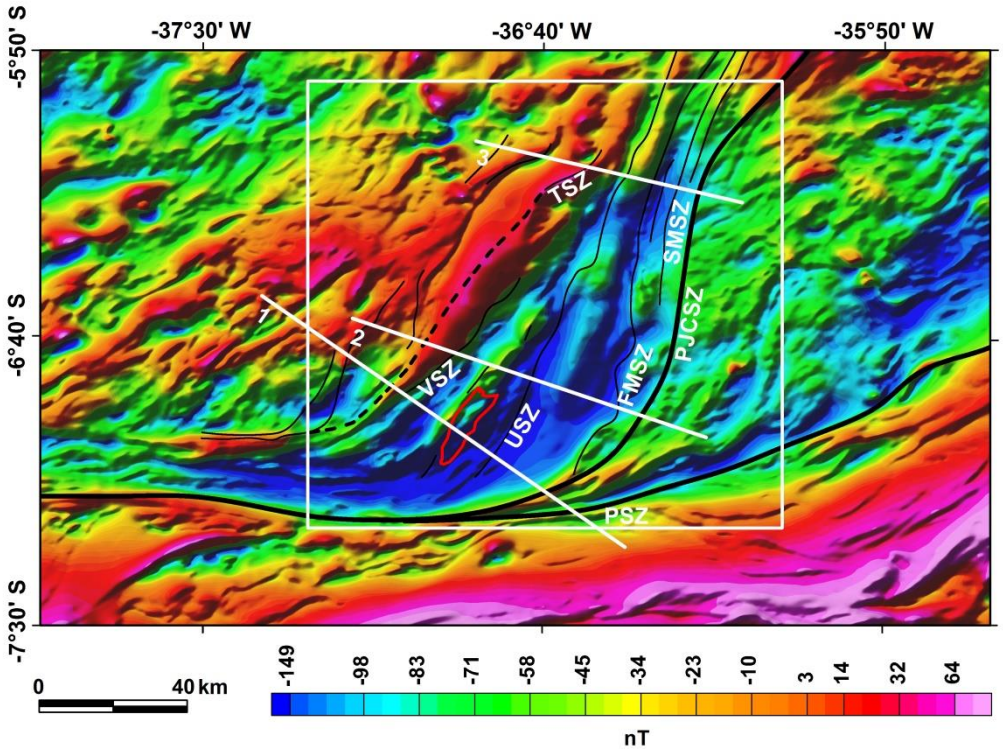


1182

1183

1184 **Figure 5**

1185

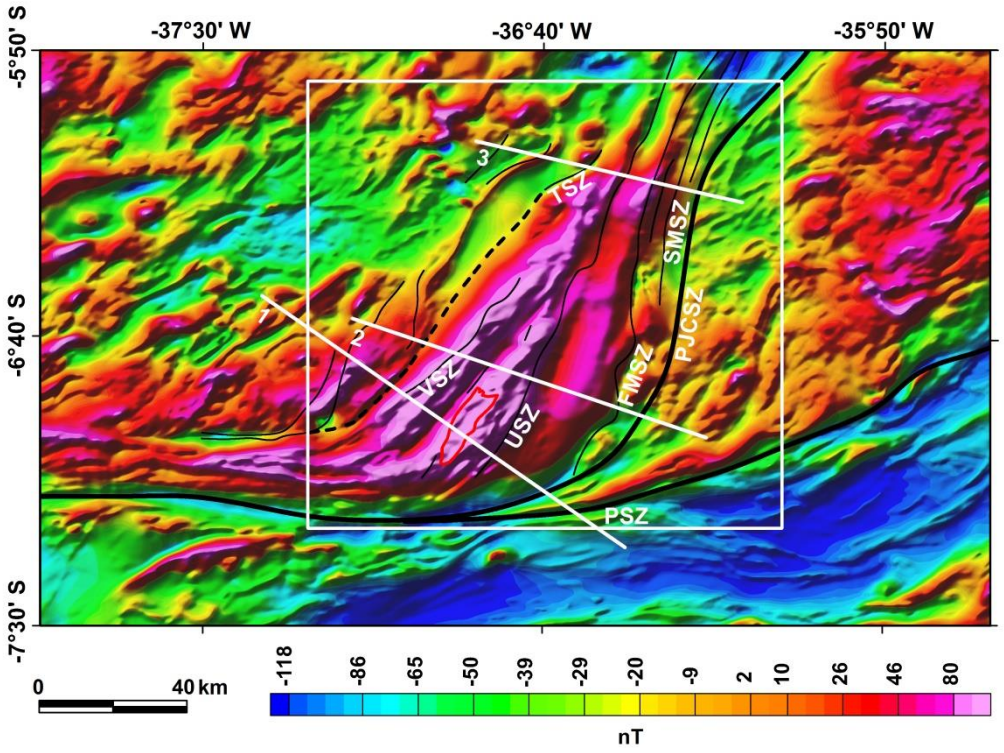


1186

1187

1188 **Figure 6**

1189

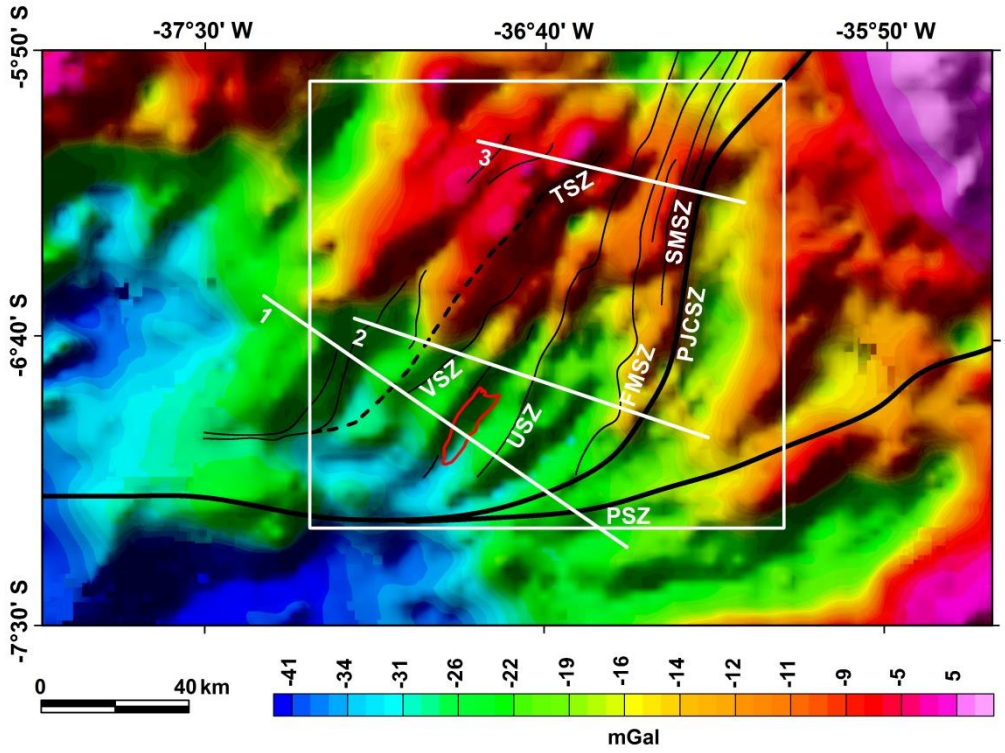


1190

1191

1192 **Figure 7**

1193

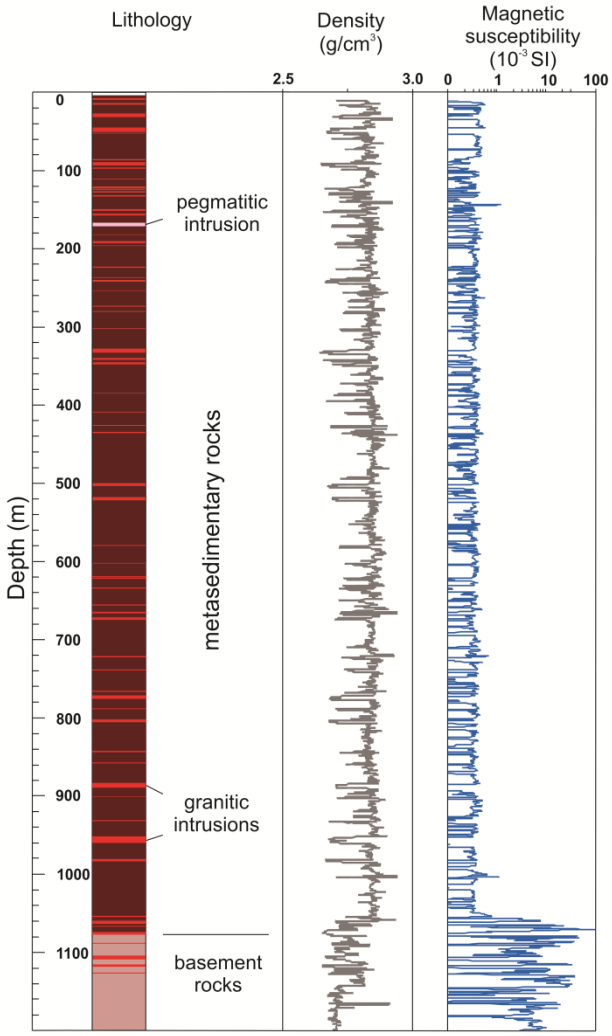


1194

1195

1196 **Figure 8**

1197

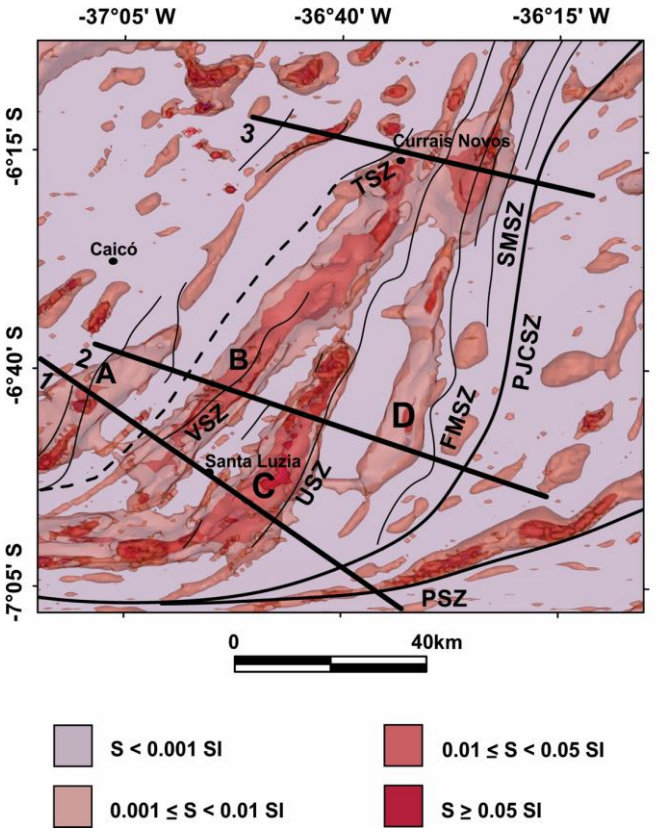


1198

1199

1200 **Figure 9**

1201

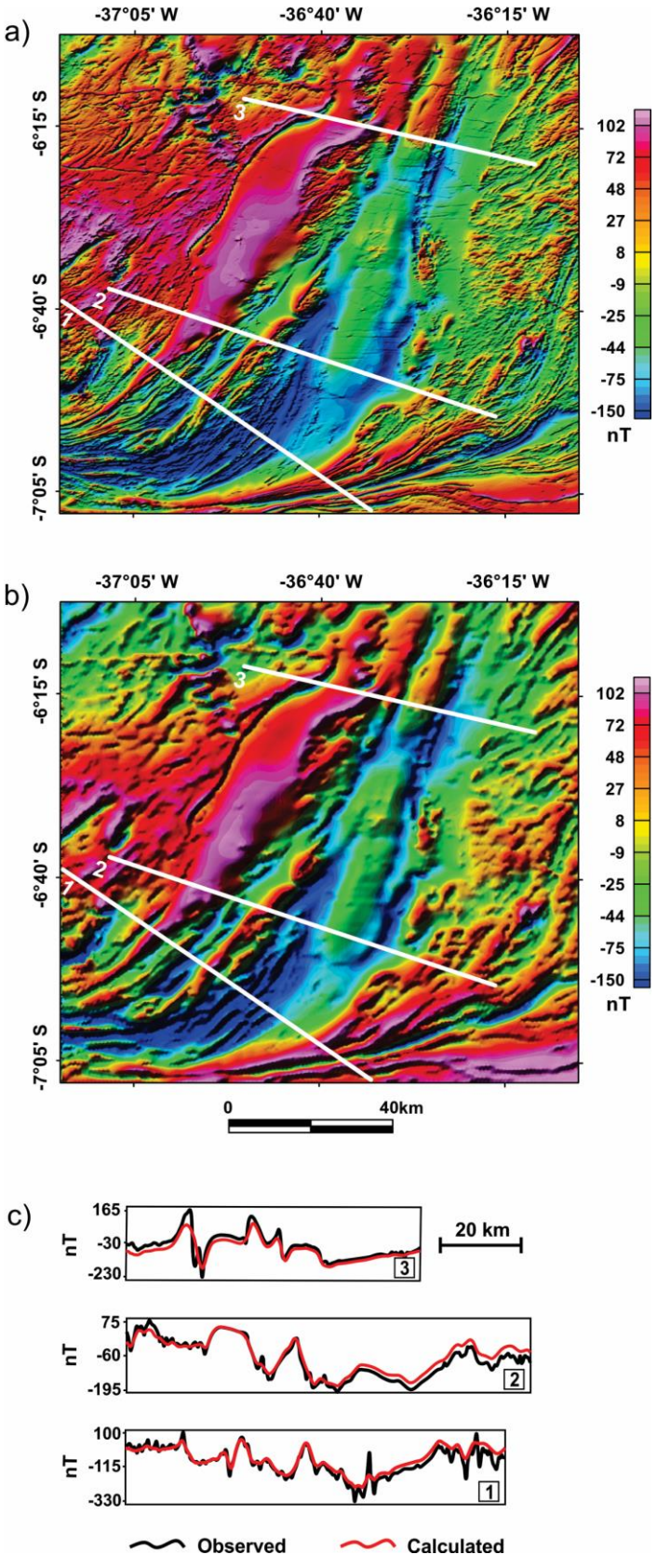


1202

1203

1204 **Figure 10**

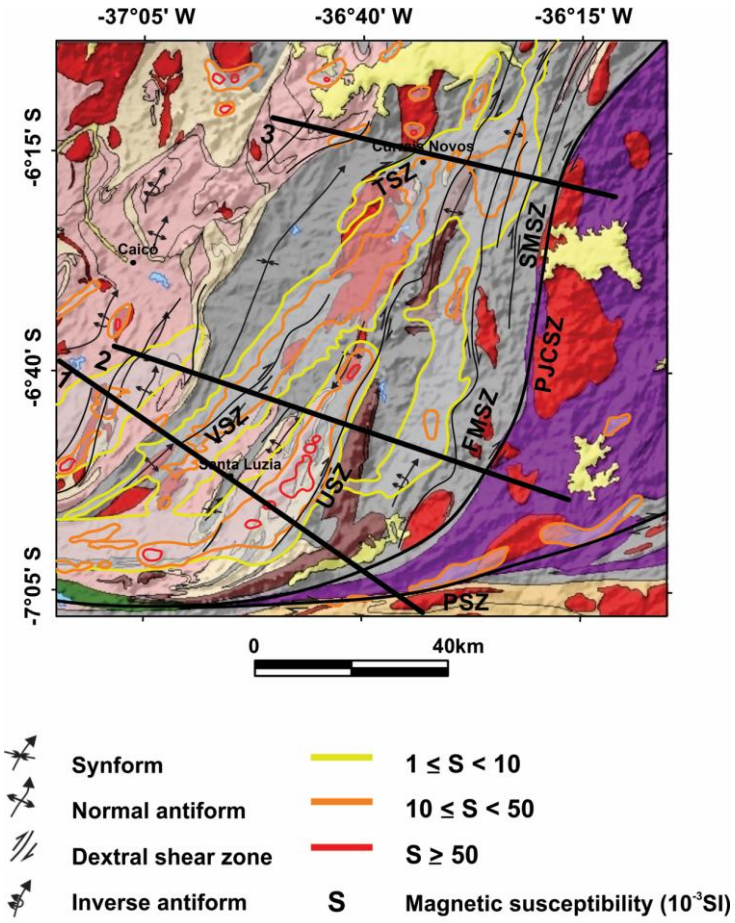


1205

1206

1207 **Figure 11**

1208

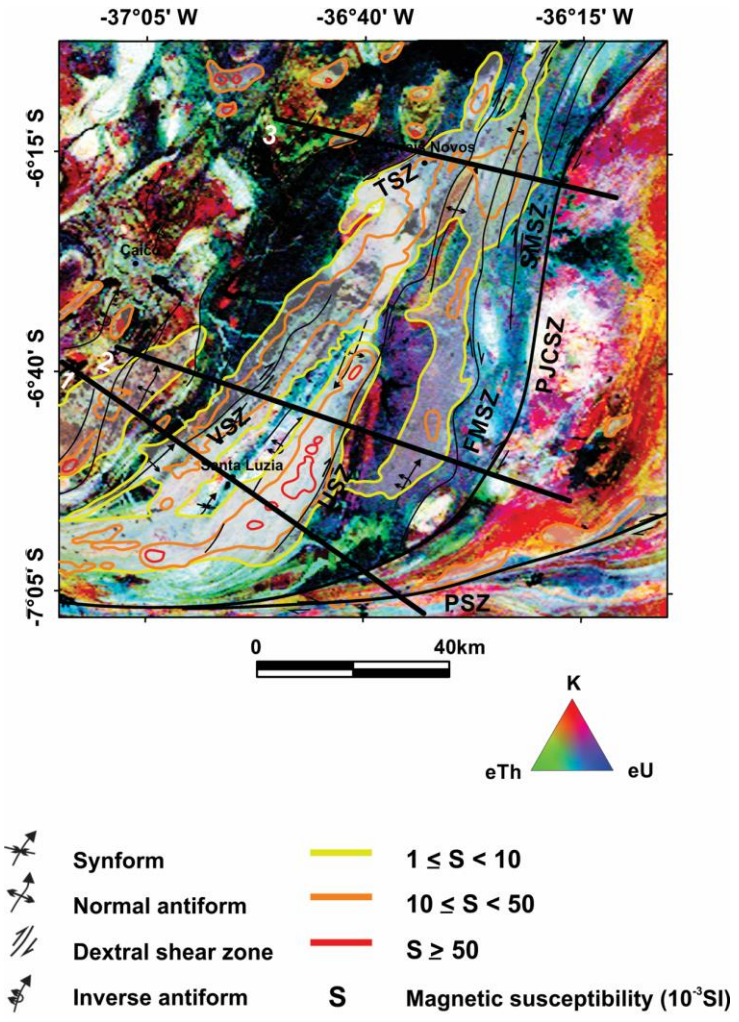


1209

1210

1211 **Figure 12**

1212

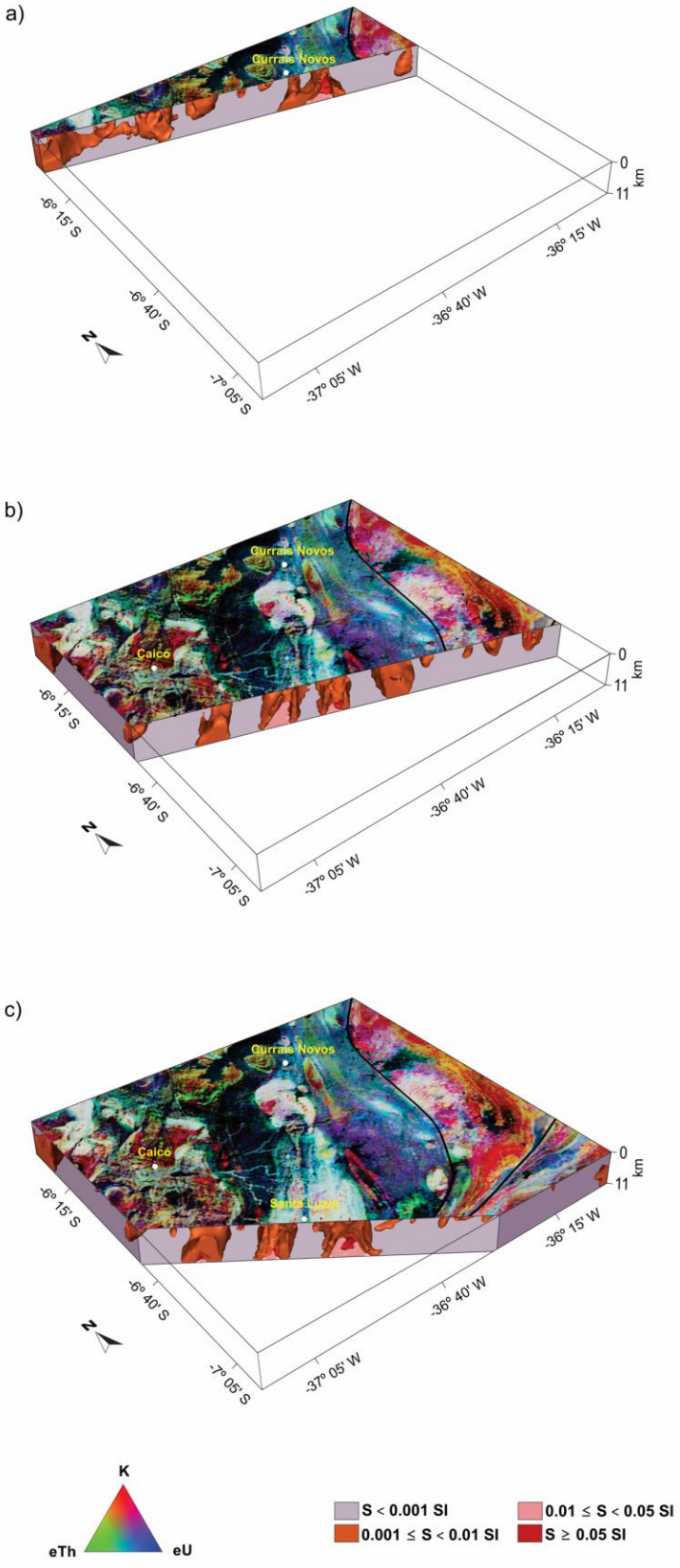


1213

1214 **Figure 13**

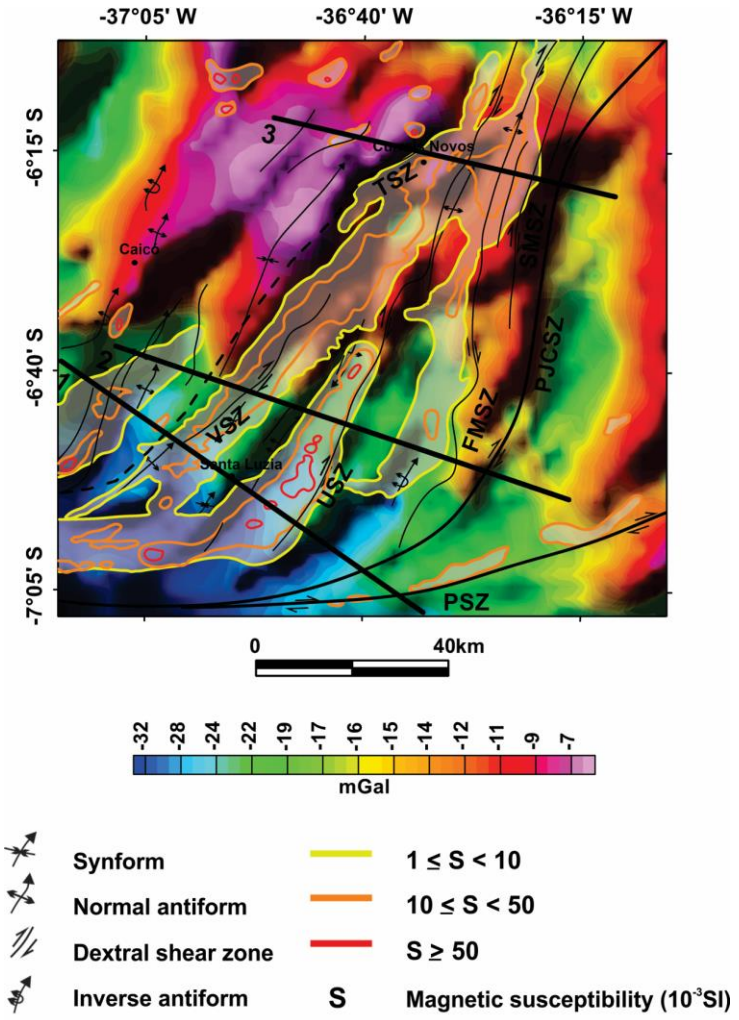
-37°05' W
-36°40' W
-36°15' W
-6°15' S
-6°40' S
-7°05' S
3
2
1
Caicó
Novos
Santa Lúcia
TSZ
SMSZ
PJCSZ
FMSZ
VSZ
USZ
PSZ
0
40km
-32
-28
-24
-22
-19
-17
-16
-15
-14
-12
-11
-9
-7
mGal
Synform
Normal antiform
Dextral shear zone
Inverse antiform
1 ≤ S < 10
10 ≤ S < 50
S ≥ 50
S
Magnetic susceptibility (10-3SI)

**Figure 14**

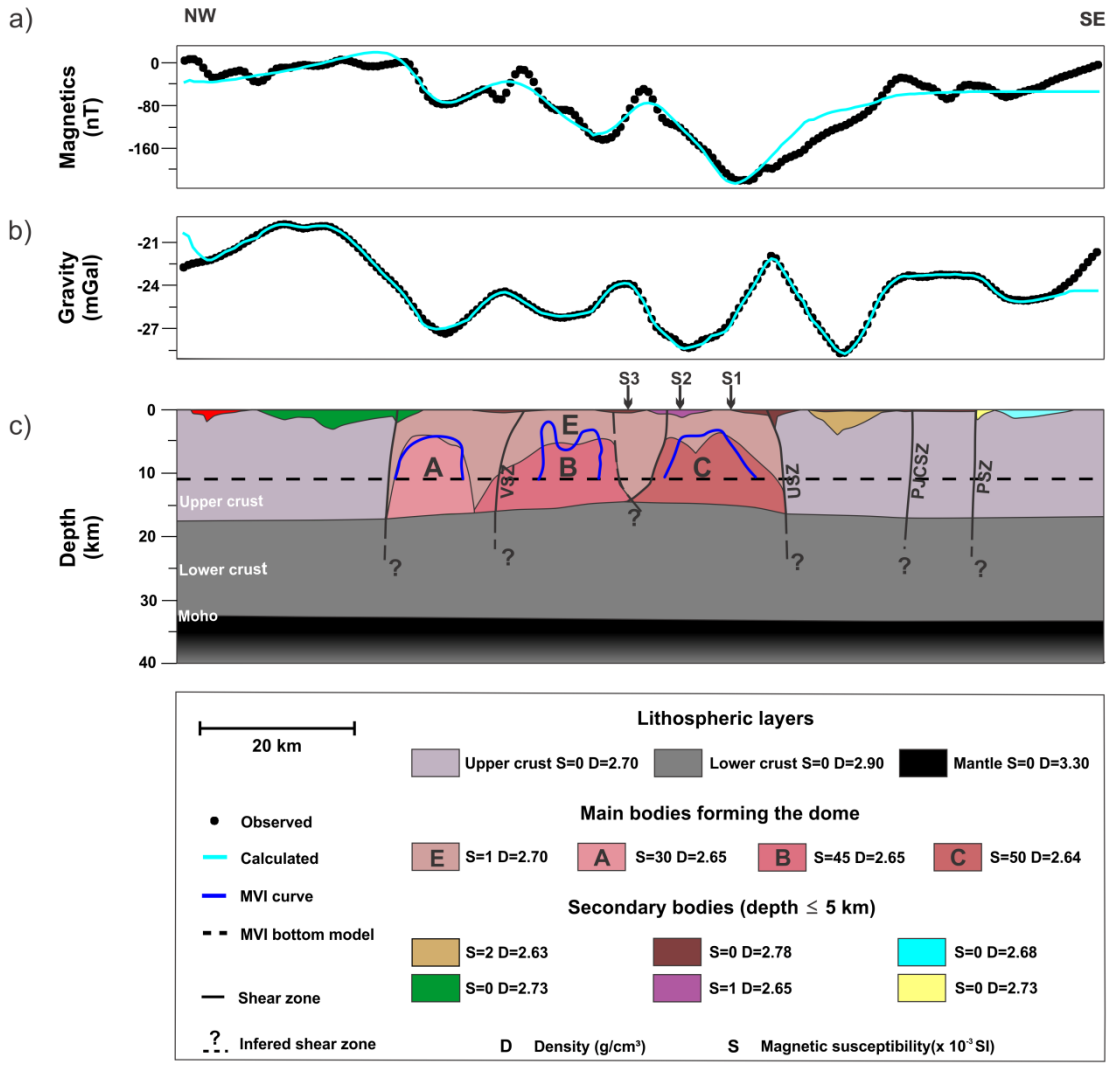
a)
NW
SE
Magnetics (nT)
0
-80
-160
b)
Gravity (mGal)
-21
-24
-27
c)
Depth (km)
S3
S2
S1
E
A
B
C
VSZ
USZ
PJCSZ
PSZ
Upper crust
Lower crust
Moho
20 km
Lithospheric layers
Upper crust S=0 D=2.70
Lower crust S=0 D=2.90
Mantle S=0 D=3.30
Observed
Calculated
MVI curve
MVI bottom model
Shear zone
Infered shear zone
Main bodies forming the dome
E S=1 D=2.70
A S=30 D=2.65
B S=45 D=2.65
C S=50 D=2.64
Secondary bodies (depth ≤ 5 km)
S=2 D=2.63
S=0 D=2.78
S=0 D=2.68
S=0 D=2.73
S=1 D=2.65
S=0 D=2.73
D Density (g/cm³)
S Magnetic susceptibility(x 10⁻³ SI)

**Figure 15**

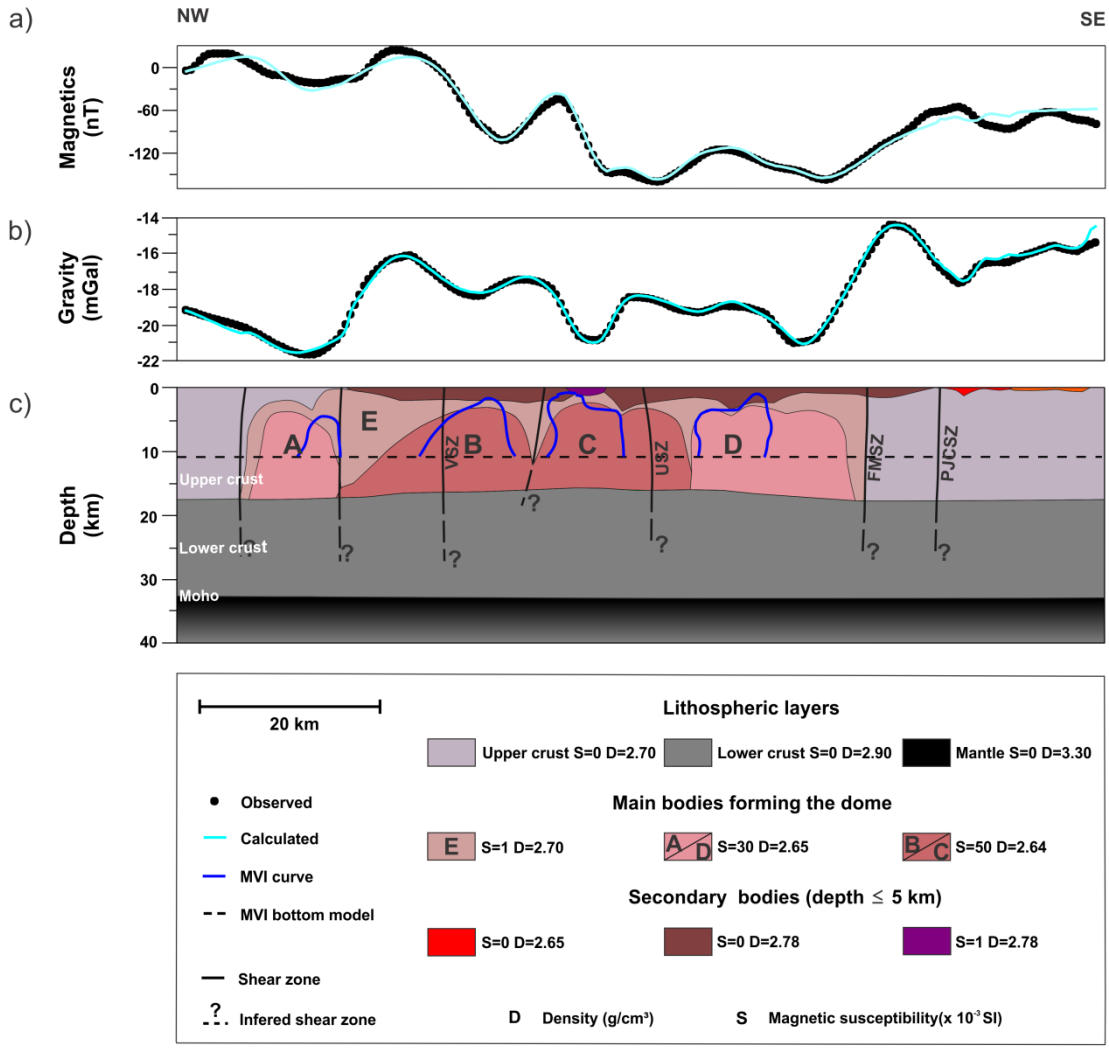
a)
NW
SE
Magnetics (nT)
0
-60
-120
b)
Gravity (mGal)
-14
-16
-18
-20
-22
c)
Depth (km)
0
10
20
30
40
A
E
B
C
D
VSZ
USZ
FMSZ
PJCSZ
Upper crust
Lower crust
Moho
?
20 km
Observed
Calculated
MVI curve
MVI bottom model
Shear zone
Infered shear zone
Lithospheric layers
Upper crust S=0 D=2.70
Lower crust S=0 D=2.90
Mantle S=0 D=3.30
Main bodies forming the dome
E S=1 D=2.70
A D S=30 D=2.65
B C S=50 D=2.64
Secondary bodies (depth ≤ 5 km)
S=0 D=2.65
S=0 D=2.78
S=1 D=2.78
D Density (g/cm³)
S Magnetic susceptibility(x 10⁻³ SI)

**Figure 16**

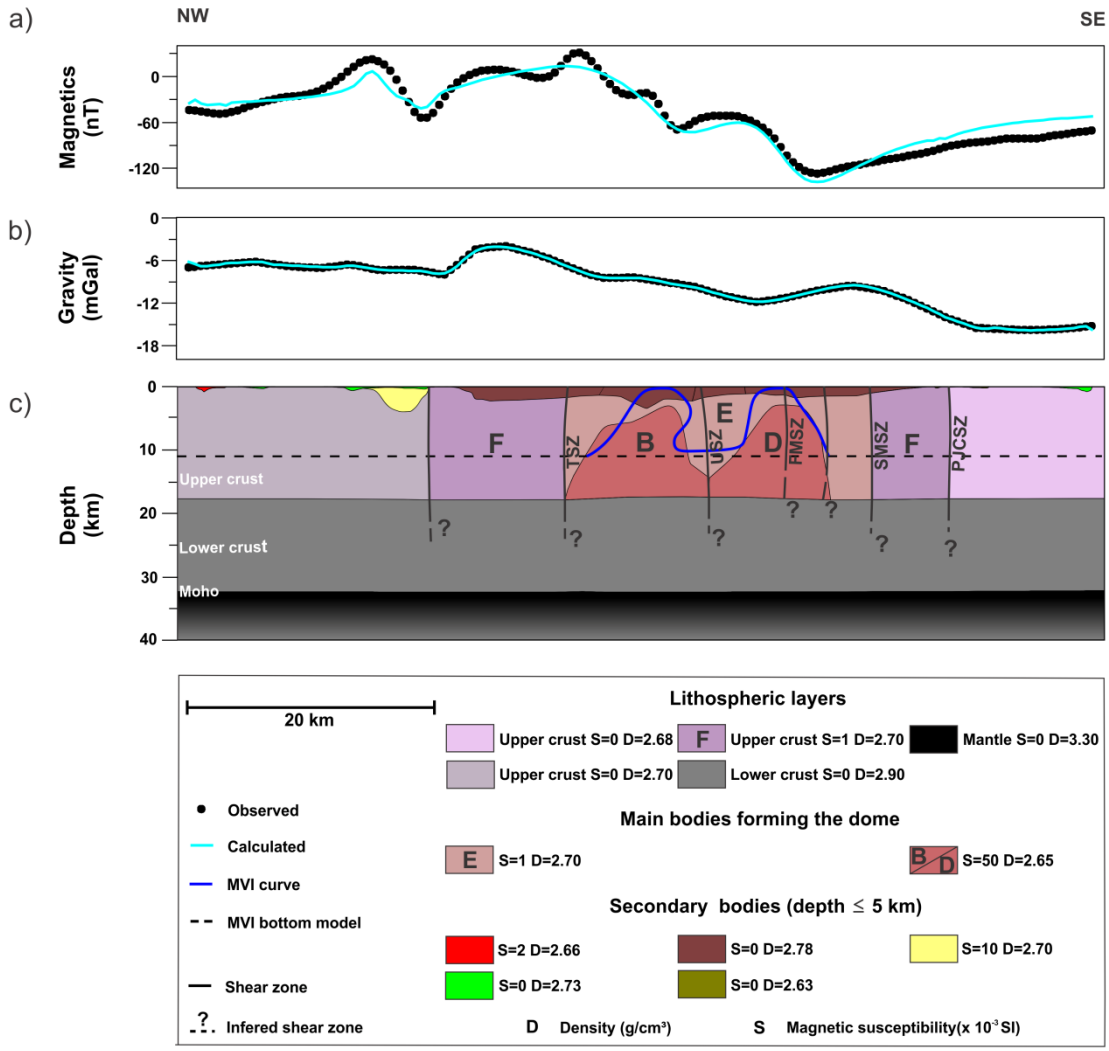
a)
NW
SE
Magnetics (nT)
0
-60
-120
b)
Gravity (mGal)
0
-6
-12
-18
c)
Depth (km)
0
10
20
30
40
Upper crust
Lower crust
Moho
F
TSZ
B
USZ
E
D
RMSZ
SMSZ
F
PJCSZ
?
20 km
Lithospheric layers
Upper crust S=0 D=2.68
F
Upper crust S=1 D=2.70
Mantle S=0 D=3.30
Upper crust S=0 D=2.70
Lower crust S=0 D=2.90
Observed
Calculated
MVI curve
MVI bottom model
Shear zone
Infered shear zone
Main bodies forming the dome
E
S=1 D=2.70
B
D
S=50 D=2.65
Secondary bodies (depth ≤ 5 km)
S=2 D=2.66
S=0 D=2.78
S=10 D=2.70
S=0 D=2.73
S=0 D=2.63
D Density (g/cm³)
S Magnetic susceptibility(x 10⁻³ SI)

**Figure 17**

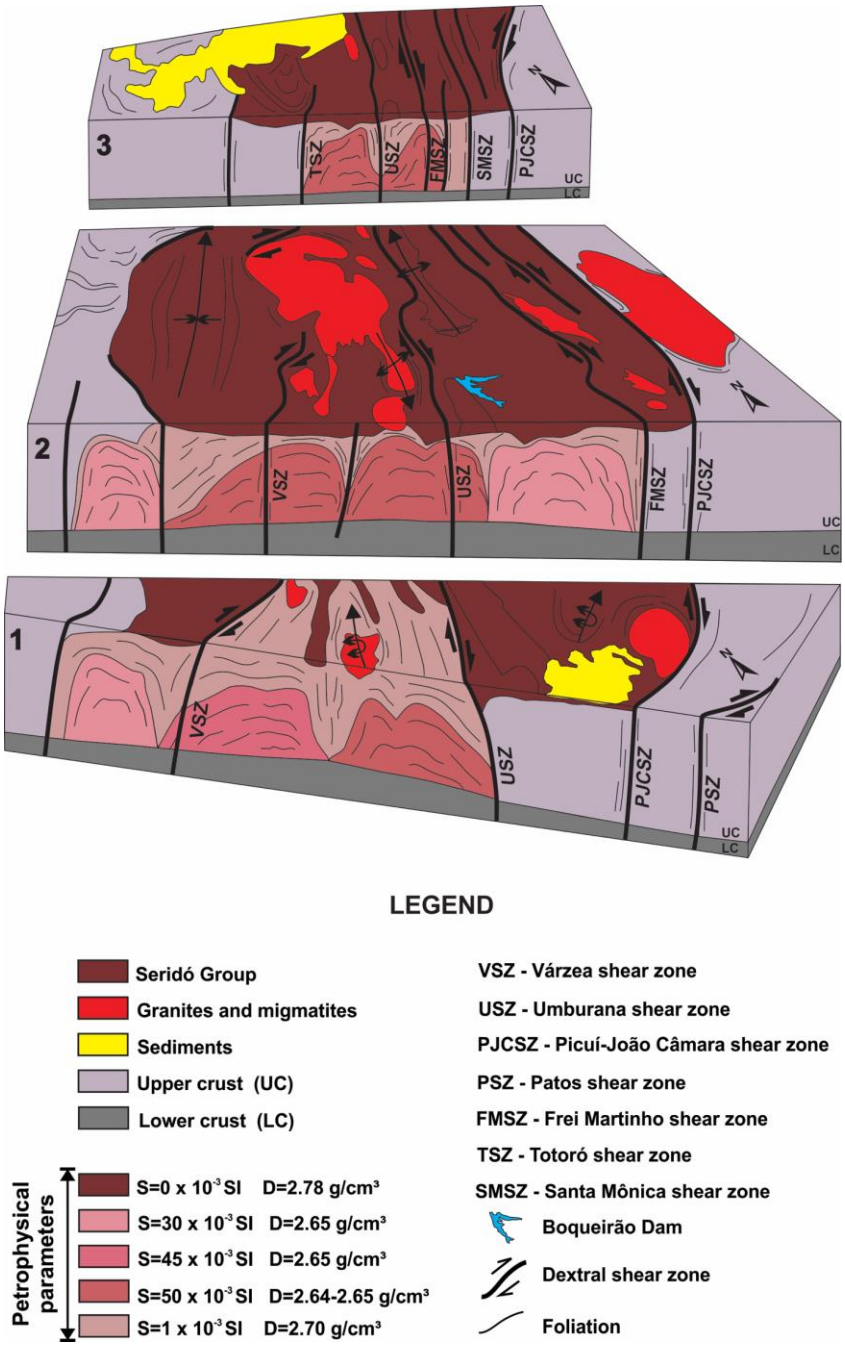


1231

1232

1233 **Figure 18**

# Capítulo 3 – Considerações finais

Os dados geofísicos magnéticos e gravimétricos evidenciam a existência de um grande volume de rochas, relativamente mais magnéticas e menos densas, na crosta superior atual da região centro-sul da Faixa Seridó. Frequentemente, zonas de cisalhamento regionais coincidem com os limites das anomalias geofísicas observadas. Essa configuração sugere que tais estruturas têm papel importante no controle tectono-estrutural das fontes causadoras das anomalias.

A interpretação qualitativa integrada dos dados geofísicos e geológicos, assim como a modelagem dos dados geofísicos, indica a presença de uma grande estrutura dômica nesta porção da Faixa Seridó. O domo regional é composto por quatro estruturas internas alongadas de direção NE-SW, que muda para E-W próximo a zona de cisalhamento Patos. Geofisicamente, as estruturas internas foram modeladas como corpos anômalos de contraste positivo de susceptibilidade magnética e contraste negativo de densidade, em relação à crosta circundante. Na modelagem geofísica, as zonas de cisalhamento serviram como limites internos e externos da estrutura dômica regional.

A correlação das anomalias geofísicas observadas com a geologia de superfície indica que as fontes causadoras são compostas por migmatitos e granitos não homogêneos ricos em magnetita. Por outro lado, os metassedimentos do Grupo Seridó ocorrem em sinformes entre as estruturas internas que compõem o domo regional. E, recobrem por completo a estrutura regional em seu segmento N-NE. A anomalia magnética de longo comprimento de onda associada à estrutura dômica principal mostra que o domo de Santa Luzia é uma estrutura de pequena escala a ela vinculada.

O processo de formação da estrutura dômica crustal na Faixa Seridó deve estar associado aos eventos tectônicos ocorridos durante a Orogênese Pan-Africana/Brasiliana,

particularmente ao escape tectônico produzido pela colisão da Província Borborema com o cráton São Francisco-Congo (Brito Neves et al., 2000; Alkmim et al., 2001; Ganade de Araújo et al., 2014).

Evidências de que a fusão parcial ocorrida a norte da zona de cisalhamento Patos, no final do Ediacarano, envolveu também os metassedimentos do Grupo Seridó são apresentadas por Cabral Neto et al. (2019) e Souza et al. (2019). Estes autores indicaram a presença de material peraluminoso onde os resultados geofísicos indicam a presença de intensa anatexia. Além disso, eles obtiveram idades U-Pb de, aproximadamente, 590 Ma para zircões de granitos peraluminosos. Estas idades são compatíveis com o pico da deformação, magmatismo e metamorfismo (~ 600 Ma) causado pela Orogênese Pan-Africana/Brasiliana (Brito Neves et al., 2014).

Cavalcante et al. (2016) sugeriram que a zona de cisalhamento Patos pode ter sido um canal para migração do material parcialmente fundido. A ocorrência de migmatitos acompanhando este lineamento crustal e, em continuidade, a porção central da Faixa Seridó (Archanjo et al., 2013; Viegas et al., 2014) fortalece a associação temporal entre migmatização na região e a atuação da zona de cisalhamento Patos como um importante limite continental transformante (Brito Neves et al., 2016) e que esta região foi uma área de intensa concentração da deformação durante a Orogênese Pan-Africana/Brasiliana.

A Faixa Seridó possui grande importância mineral. A área apresenta diversos tipos de depósitos minerais metálicos, não metálicos, gemas e metais preciosos, com potencialidade para tungstênio, molibdênio, ouro, cobre, ferro, tântalo, e nióbio, entre outros. Ela abrange duas principais províncias minerais do nordeste do Brasil: a Província Mineral do Seridó e a Província Pegmatítica da Borborema. As zonas de cisalhamento, os sistemas de fraturas a elas relacionados, a percolação de fluidos hidrotermais

resultantes do magmatismo granítico e o metamorfismo regional contribuíram para a importante vocação mineira da região (Salim, 1993).

Dados das ocorrências minerais da Faixa Seridó mostram uma boa correspondência espacial com as zonas de migmatização indicadas pelos resultados apresentados. Considerando a importância mineral da área, é necessário melhor compreender como as zonas de cisalhamento e os fluidos oriundos da migmatização e das injeções magmáticas ocorridas no Ediacarano influenciaram a ocorrência e distribuição dos depósitos minerais (migração de fluidos, resfriamento de materiais e distribuição das massas) na área.

Uma característica interessante dos migmatitos e granitos que ocorrem associados à estrutura dômica regional é a presença expressiva de magnetitas (inclusive cristais centimétricos). As magnetitas presentes contribuem para o aumento da susceptibilidade magnética destas rochas e, consequentemente, para a intensa anomalia magnética que ocorre associada à presença do domo. Por isso, um outro aspecto importante a ser retratado em trabalhos futuros é a discussão da proveniência das magnetitas em termos da evolução tectônica da região.

# Referências bibliográficas

Alkmim, F.F., Marshak, S., Fonseca, M.A., 2001. Assembling West Gondwana in the Neoproterozoic: clues from the São Francisco craton region, Brazil. Geology 29, 319–322.https://doi.org/10.1130/0091-7613(2001)029<0319:AWGITN>2.0.CO;2.

Almeida, F.F.M., Hasui, Y., Brito Neves, B.B., Fuck, R.A., 1981. Brazilian structural provinces: an introduction. Earth-Sci. Rev. 17 (1-2), 1-29. https://doi.org/10.1016/0012-8252(81)900039.

Angelim, L.A.A., Vasconcelos, A.M., Gomes, J.R.C., Wanderley, A.A., Forgiarini, L.L., Medeiros, M. de F., 2004. Folha SB.24-Jaguaribe. In: Schobbenhaus, C., Gonçalves, J.H., Santos, J.O.S., Abram, M.B., Leão Neto, R., Matos, G.M.M., Vidotti, R.M., Ramos, M.A.B., Jesus, J.D.A. de (Eds.). Carta Geológica do Brasil ao Milionésimo. Sistema de Informações Geográficas - SIG, Programa Geologia do Brasil. CPRM, Brasília, CD-ROM. http://www.cprm.gov.br/publique/Geologia/Geologia-Basica/Carta-Geologica-do-Brasil-ao-Milionesimo-298.html (accessed 21 October 2019).

Archanjo, C.J., Hollanda, M.H.B.M., Rodrigues, S.W.O., Brito Neves, B.B., Armstong, R., 2008. Fabrics of pre- and syntectonic granite plutons and chronology of shear zones in the Eastern Borborema Province, NE Brazil. J. Struct. Geol. 30 (3), 310-336. https://doi.org/10.1016/j.jsg.2007.11.011.

Archanjo, C.J., Viegas, L.G., Hollanda, M.H.B.M., Souza, L.C., Liu, D., 2013. Timing of the HT/LP transpression in the Neoproterozoic Seridó Belt (Borborema Province, Brazil): Constraints from U-Pb (SHRIMP) geochronology and implications for the connections between NE Brazil and West Africa. Gondwana Res. 23 (2), 701-714. https://doi.org/10.1016/j.gr.2012.05.005.

Ayarza, P., Martínez Catalán, J.R., 2007. Potential field constraints on the deep structure of the Lugo gneiss dome (NW Spain). Tectonophysics. 439 (1-4), 67-87. https://doi.org/10.1016/j.tecto.2007.03.007.

Baldim, M.R., Oliveira, E.P., 2016. Anatomy of the Alto Alegre gneiss dome, São Francisco Craton, Brazil: A geological record of transpression along a Paleoproterozoic arc-continent collision zone. Precambrian Res. 286, 250-268. https://doi.org/10.1016/j.precamres.2016.10.004.

Beltrão, J. F., Silva, J. B. C., Costa, J. C., 1991. Robust polynomial fitting method for regional gravity estimation. Geophysics, 56: 80-89. https://doi.org/10.1190/1.1442960

Blakely, R.J., 1995. Potential Theory in Gravity and Magnetic Applications. Cambridge: Cambridge University Press. 441 pp. https://doi.org/10.1017/CBO9780511549816.

Brito Neves, B.B., Cordani, U.G., 1991. Tectonic evolution of South America during the Late Proterozoic. Precambrian Res. 53 (1-2), 23-40. https://doi.org/10.1016/0301-9268(91)90004-T.

Brito Neves, B.B., Santos, E.J., Van Schmus, W.R., 2000. Tectonic history of the Borborema Province, NW Brazil. In: Cordani, U.G., Milani, E.J., Thomaz-Filho, A., Campos, D.A. (Eds.), Tectonic Evolution of South America. 31st International Geological Congress, Rio de Janeiro, pp. 151–182.

Brito Neves, B.B., Fuck, R.A., Pimentel, M.M., 2014. The Brasiliano collage in South America: a review. Braz. J. Geol. 44 (3), 493–518. http://dx.doi.org/10.5327/Z2317-4889201400030010.

Brito Neves B.B., Santos E.J., Fuck R.A., Santos L.C.M.L., 2016. A preserved early Ediacaran magmatic arc at the northernmost portion of the Transversal Zone central subprovince of the Borborema Province, Northeastern South America. *Brazilian Journal of Geology*, 46, 491-508. http://dx.doi.org/10.1590/2317-4889201620160004.

Brown, R.L., Journeay, J.M., Lane, L.S., Murphy, D.C., Rees, C.J., 1986. Obduction, backfolding and piggyback thrusting in the metamorphic hinterland of the southeastern Canadian Cordillera. J. Struct. Geol. 8 (3-4), 225-268. https://doi.org/10.1016/0191-8141(86)900477.

Brun, J.P., 1983. L'origine des domes gneissiques: Modeleset tests. Bull. Soc. Geol. Fr. 25, 219-228. https://doi.org/10.2113/gssgfbull.S7-XXV.2.219.

Cabral Neto, I., de Medeiros, V., Cavalcante, R., Fernandes, P., Silveira, F., Dantas, E., Rodrigues, J., Cunha, I., Paes, V., Santos, L., Pinho, I., 2019. Jardim do Seridó Suite: first example of Ediacaran peraluminous magmatism in the Rio Piranhas-Seridó Domain, Borborema Province, Northeast Brazil. J. Geol. Surv. Braz. 2 (2), 119-136. https://doi.org/10.29396/jgsb.2019.v2.n2.3.

Caby, R., Arthaud, M.H., 1986. Major Precambrian nappes of the Brazilian belts, Ceará, Northeast Brazil. Geology. 14 (10), 871–874. https://doi.org/10.1130/0091-7613(1986)14<871:MPNOTB>2.0.CO;2.

Caby, R., Sial, A.N., Arthaud, M.H., Vauchez, A., 1991. Crustal evolution and the Brasiliano orogeny in northeast Brazil. In: Dallmeyer, R.D., Lé corché, J.P. (Eds.), The West African Orogens and Circum-Pacific-Atlantic Correlatives. Springer, Berlin, Heidelberg, pp. 373–397. https://doi.org/10.1007/978-3-642-84153-8_16.

Cavalcante, G.C.G., Viegas, G., Archanjo, C.J., Silva, M. E., 2016. The influence of partial melting and melt migration on the rheology of the continental crust. J. Geodyn. 101, 186-199. https://doi.org/10.1016/j.jog.2016.06.002.

Caxito, F.A., Uhlein, A., Dantas, E.L., Stevenson, R., Salgado, S.S., Dussin, A.I., Sial, A.N., 2016. A complete Wilson Cycle recorded within the Riacho do Pontal Orogen, NE Brazil: implications for the Neoproterozoic evolution of the Borborema Province at the heart of West Gondwana. Precambrian Res. 282, 97-120. https://doi.org/10.1016/j.precamres.2016.07.001.

Constable, S.C., Parker, R.L., Constable, C.G., 1987. Occam's inversion: A practical algorithm for generating smooth models from electromagnetic sounding data. Geophysics. 52 (3), 289-300. http://dx.doi.org/10.1190/1.1442303.

Corsini, M., Vauchez, A., Archanjo, C.J., Jardim de Sá, E.F., 1991. Strain transfer at a continental scale from a transcurrent shear zone to a transpressional fold belt: the Patos-Seridó belt system,

north-eastern Brazil. Geology. 19 (6), 586-589. https://doi.org/10.1130/0091-7613(1991)019%3C0586:STACSF%3E2.3.CO;2.

Corsini, M., Lambert De Figueiredo, L., Caby, R., Féraud, G., Ruffet, G., Vauches, A., 1998. Thermal history of the Pan/African – Brasiliano Borborema province of the northeast Brazil, deduced from 40AR/39AR analysis. Tectonophysics. 285 (1-2), 103-117. https://doi.org/10.1016/S0040-1951(97)00192-3.

Crowley, J.L., Brown, R.L., Parrish, R.R., 2001. Diachronous deformation and a strain gradient beneath the Selkirk allochthon, northern Monashee complex, southeastern Canadian Cordillera. J. Struct. Geol. 23 (6-7), 1103-1121. https://doi.org/10.1016/S0191-8141(00)00179-6.

Cunningham, D., 2010. Tectonic setting and structural evolution of the late Cenozoic Gobi Altai orogen. In: Kusky, T.M., Zhai, M.G., Xiao, W.J. (Eds.), The Evolving Continents: Understanding Processes of Continental Growth and Stabilization, Geol. Soc. Lond. Spec. Publ. 338 (1), pp. 361-387. http://dx.doi.org/10.1144/SP338.17.

Cutts, K., Lana, C., Alkmim, F., Farina, F., Moreira, H., Coelho, V., 2019. Metamorphism and exhumation of basement gneiss domes in the Quadrilátero Ferrífero: Two stage dome-and-keel evolution? Geosci. Front. 10 (5), 1765-1787. https://doi.org/10.1016/j.gsf.2019.02.009.

Dantas, E.L., 1992. Evolução tectono-magmática do maciço polidiapírico São Vicente-Florânia – RN. Dissertação de mestrado, Universidade Estadual Paulista, Instituto de Geociências e Ciências Exatas, pp. 272.

Dantas, E.L., 1997. Geocronologia U-Pb e Sm-Nd de terrenos arqueanos e paleoproterozóicos do Maciço Caldas Brandão, NE do Brasil. Tese de doutorado, Universidade Estadual Paulista, Instituto de Geociências e Ciências Exatas, pp. 206.

D'el-Rey Silva, L.J.H., 1995. The evolution of basement gneiss domes of the Sergipano fold belt (NE Brazil) and its importance for the analysis of Proterozoic basins. J. S. Am. Earth Sci. 8 (3-4). 325-340. https://doi.org/10.1016/0895-9811(95)00017-A.

Dixon, J.M., 1987. Mantled gneiss domes. In: Structural Geology and Tectonics. Encyclopedia of Earth Science. Springer, Berlim, Heidelberg.

Domingos, N. R. R., Oliveira, R. G., Rodrigues, M. A. C., Silva, E. P. 2017. Levantamento Gravimétrico da Faixa Seridó (NE-Brasil): Implicações para o Mapeamento Geológico e o Arcabouço Tectônico. *In:* XV Congr. Bras. SBGf, Rio de Janeiro.

Ellis, R.G., Wet, B., Macleod, I.N., 2012. Inversion of magnetic data from remanent and induced sources. In: 22nd Annual Australian Society of Exploration Geophysicists Conference and Exhibition, Brisbane, Electronic Abstracts, 1-4. https://doi.org/10.1071/ASEG2012ab117.

Eskola, P.E., 1949. The problem of mantled gneiss domes. Quart. J. Geol. Soc. London. 104, 461-476. https://doi.org/10.1144/GSL.JGS.1948.104.01-04.21.

Fletcher, R.C., 1972. Application of a mathematical model to the emplacement of mantled gneiss domes. Am. J. Sci. 272 (3), 197–216. https://doi.org/10.2475/ajs.272.3.197.

Ganade de Araújo, C.E., Weinberg, R.F., Cordani, U.G., 2014. Extruding the Borborema Province (NE-Brazil): a two-stage Neoproterozoic collision process. Terra Nova. 26, 1–12. https://doi.org/10.1111/ter.12084.

Grujic, D., 2006. Channel flow and continental collision tectonics: An overview. In: Law, R.D., Searle, M.P., Godin, L. (Eds.), Channel Flow, Ductile Extrusion and Exhumation in Continental Collision Zones, Geol. Soc. Lond. Spec. Publ. 268, pp. 25-75. http://dx.doi.org/10.1144/GSL.SP.2006.268.01.02.

Hollanda, M.H.B.M., Archanjo, C.J., Bautista, J.R., Souza, L.C., 2015. Detrital zircon ages and Nd isotope compositions of the Seridó and Lavras da Mangabeira basins (Borborema Province, NE Brazil): evidence for exhumation and recycling associated with a major shift in sedimentary provenance. Precambr. Res. 258, 181–207. https://doi.org/10.1016/j.precamres.2014.12.009.

Jamieson, R.A., Beaumont, C., Nguyen, M.H., Grujic, D., 2006. Provenance of the Greater Himalayan Sequence and associated rocks: predictions of channel flow models. In: Law, R.D., Searle, M.P., Godin, L. (Eds.), Channel Flow, Ductile Extrusion and Exhumation in Continental Collision Zones, Geol. Soc. Lond. Spec. Publ. 268, pp. 165-182. http://dx.doi.org/10.1144/GSL.SP.2006.268.01.07.

Jamieson, R.A., Unsworth, M.J., Harris, N.B.W., Rosenberg, C.L., Schulmann, K., 2011. Crustal melting and the flow of mountains. Elements. 7 (4), 253-260. https://doi.org/10.2113/gselements.7.4.253.

Jardim de Sá, E.F., 1994. A faixa Seridó (província Borborema, NE do Brasil) e seu significado geodinâmico na cadeia brasiliana/pan-africana. Tese de doutorado, Universidade de Brasília, Instituto de Geociências, Brasília, pp. 804.

Kodama, K.P., Chapin, D.A., 1984. A detailed gravity study of the Chattolanee Beltimore Gneiss Dome, Maryland, U.S.A. Earth Planet. Sci. Lett. 68 (2), 286-296. https://doi.org/10.1016/0012-821X(84)90160-2.

Kruckenberg, S.C., Vanderhaeghe, O., Ferré, E.C., Teyssier, C., Whitney, D.L., 2011. Flow of partially molten crust and the internal dynamics of a migmatite dome. Naxos, Greece. Tectonics. 30 (3), TC3001. https://doi.org/10.1029/2010TC002751.

Lasa Engenharia e Prospecções S.A. & Prospectors Aerolevantamentos e Sistemas Ltda. 2008. Projeto Levantamento Aerogeofísico Borda Leste do Planalto da Borborema. Ministério de Minas e Energia, Secretaria de Geologia, Mineração e Transformação Mineral, CPRM – Serviço Geológico do Brasil, Relatório Final, Texto e Anexos (Mapas), Rio de Janeiro, pp. 401.

Lasa Engenharia e Prospecções S.A. & Prospectors Aerolevantamentos e Sistemas Ltda. 2010. Projeto Aerogeofísico Paraíba-Rio Grande do Norte e Pernambuco-Paraíba. Texto Técnico, Rep. Fed. Do Brasil, MME/Secretaria de Geologia, Mineração e Transformação Mineral/CPRM-Serviço Geológico do Brasil, pp. 389.

Li, Z.X., Bogdanova, S.V., Collins, A.S., Davidson, A., De Waele, B., Ernst, R.E., Fitzsimons, I.C.W., Fuck, R.A., Gladkochub, D.P., Jacobs, J., Karlstrom, K.E., Lu, S., Natapov, L.M., Pease, V., Pisarevsky, S.A., Thrane, K., Vernikovsky, V., 2008. Assembly, configuration, and break-up history of Rodinia: a synthesis. Precambr. Res. 160, 171–210. https://doi.org/10.1016/j.precamres.2007.04.021.

Lima, E.S., 1987. Evolução termo-barométrica das rochas metapelíticas da região do Seridó, Nordeste Brasileiro. Rev. Bras. Geoc. 17 (3), 315–323. https://doi.org/10.25249/0375-7536.1987315323.

Lima, M.V.A.G., Berrocal, J., Soares, E.P., Fuck, R.A., 2015. Deep seismic refraction experiment in northeast Brazil: new constraints for Borborema province evolution. J. S. Am. Earth Sci. 58, 335-349. https://doi.org/10.1016/j.jsames.2014.10.007.

Luz, R.M.N., Julià, J., Do Nascimento, A.F., 2015. Crustal structure of the eastern Borborema Province, NE Brazil, from the joint inversion of receiver functions and surface wave dispersion: Implications for plateau uplift, J. Geophys. Res. Solid Earth, 120, 3848-3869. https://doi.org/10.1002/2015JB011872.

MacLeod, I.N., Ellis, R.G., 2013. Magnetic Vector Inversion, a simple approach to the challenge of varying direction of rock magnetization. In: ASEG Forum on the Application of Remanent Magnetization. ASEG, 1-4, Melbourne, Australia.

MacLeod, I.N., Ellis, R.., 2016. Quantitative magnetization vector inversion. In: 25th Geophysical Conference & Exhibition. ASEG-PESA-AIG,1-5, Adelaide, Australia.

Magini, C., Hackspacher, P.C., Legrand, J.M., Neves, B.B.B., Petta, R.A., Sial, A.N., Dantas, E.L., 1997. Proterozoic tectono-metamorphic evolution of the SãoVicente-Caicó batolith (State of Rio Grande do Norte). Rev. Bras. Geociências 16, 257-277.

Martínez Catalán, J.R., Ayarza, P., Álvarez Lobato, F., Villalaín, J.J., Durán Oreja, M., Martín Paramio, M., Rodríguez Gómez, S., 2018. Magnetic anomalies in extensional detachments: The

Xistral Tectonic Window of the Lugo Dome (NW Spain). Tectonics. 37 (11), 4261–4284. https://doi.org/10.1029/2017TC004887.

Medeiros, V.C., Cavalcante, R., Cunha, A.L.C., Dantas, A.R., Costa, A.P., Brito, A.A., Rodrigues, J.B., Silva, M.A., 2017. O furo estratigráfico de Riacho Fechado (Currais Novos/RN), Domínio Rio Piranhas-Seridó (Província Borborema, NE do Brasil): Procedimentos e resultados. Estudos Geológicos (UFPE), 27 (3), 3-44.

Minty, B.R.S., 1997. The fundamentals of airborne gammaray spectrometry. J. Aust. Geol. Geophys. 17 (2), 39-50.

Moreira, J.A.M., Medeiros, W.E., Lins, F.A.P.L., Archanjo, C.J., 1989. Uma anomalia magnética de caráter regional no Seridó (RN-PB) e uma discussão de sua origem. In: I Congr. Bras. SBGf, 592-597, Rio de Janeiro-RJ.

Nelson, K.D., Zhao, W., Brown, L.D., Kuo, J., Che, J., Liu, X., Klemperer, S.L., Makovsky, Y., Meissner, R., Mechie, J., Kind, R., Wenzel, F., Ni, J., Nabelek, J., Leshou, C., Tan, H., Wei, W., Jones, A.G., Booker, J., Unsworth, M., Kidd, W.S.F., Hauck, M., Alsdorf, D., Ross, A., Cogan, M., Wu, C., Sandvol, E., and Edwards, M., 1996, Partially molten middle crust beneath southern Tibet: A synthesis of Project INDEPTH results: Science, v. 274, p. 1684–1688, doi:10.1126 /science.274.5293.1684.

Neves, S.P., Vauchez, A., Feraud, G., 2000. Tectono-thermal evolution, magma emplacement, and shear zone development in the Caruaru area (Borborema Province, NE Brazil). Precambrian Res. 99 (1-2), 1–32. https://doi.org/10.1016/S0301-9268(99)00026-1.

Neves, S.P., Monié, P., Bruguier, O., Rangel da Silva, J.M., 2012. Geochronological, thermochronological and thermobarometric constraints on deformation, magmatism and thermal regimes in eastern Borborema Province (NE Brazil). J. S. Am. Earth Sci. 38, 129-146. https://doi.org/10.1016/j.jsames.2012.06.003.

Oliveira, E.P., McNaughton N.J., Windley, B.F., Carvalho, M.J., Nascimento, R.S., 2015. Detrital zircon U-Pb geochronology and whole-rock Nd-isotope constraints on sediment provenance in the Neoproterozoic Sergipano orogen, Brazil: From early passive margins to late foreland basins. Tectonophysics. 662, 183-194. https://doi.org/10.1016/j.tecto.2015.02.017.

Oliveira, R. G. 2008. Arcabouço geofísico, isostasia e causas do magmatismo cenozóico da Província Borborema e de sua margem continental (Nordeste do Brasil). Tese de doutorado, Universidade Federal do Rio Grande do Norte, Natal, pp. 411.

Oliveira, R.G., Medeiros, W.E., 2012. Evidences of buried loads in the base of the crust of Borborema Plateau (NE Brazil) from Bouguer admittance estimates. J. S. Am. Earth Sci. 37, 60–76. https://doi.org/10.1016/j.jsames.2012.02.004.

Oliveira, R.G., Medeiros, W.E., 2018. Deep crustal framework of the Borborema Province, NE Brazil, derived from gravity and magnetic data. Precambrian Res. 315, 45-65. https://doi.org/10.1016/j.precamres.2018.07.004.

Osako, L.S., Castro, D.L. de,Fuck, R.A., Castro, N.A., Pitombeira, J.P.A., 2011. Contribuição de uma seção gravimétrica transversal ao estudo da estruturação litosférica na porção setentrional da Província Borborema, NE do Brasil. Rev. Bras. Geof. 29 (2), 309-329. http://dx.doi.org/10.1590/S0102-261X2011000200008.

Rizzotto, G.J., Alves, C.L., Rios, F.S., Barros, M.A.S., 2019. The Nova Monte Verde metamorphic core complex: Tectonic implications for the southern Amazonian craton. J. S. Am. Earth Sci. 91, 154-172. https://doi.org/10.1016/j.jsames.2019.01.003.

Salim, José. Geologie, petrologie et geochimie des skarns a scheelite de la Mine Brejui, Currais Novos, Region du Serido, NE du Bresil. Louvain-La-Neuve, 1993. 272 p. Thèse ( Docteur en Sciences) - Laboratoire de Géologie et Minéralogie, Universite Catholique de Louvain, Belgique, 1993.

Searle, M.P., Treloar, P.J., 2019. Himalayan Tectonics: A Modern Synthesis. Geol. Soc. Lond. Spec. Publ. 483, 1–17. https://doi.org/10.1144/SP483-2019-20.

Sial, A.N. 1986. Granite types in Northeastern Brazil. Current knowledge. Rev. Bras. Geoc. 16 (1), 54-72. https://doi.org/10.25249/0375-7536.19865472.

Silva, J.B.C., Barbosa, V.C.F., Medeiros, W.E., 2002, Practical applications of uniqueness theorems in Gravimetry. Part II - Pragmatic incorporation of concrete geologic information: Geophysics, 67: 795 – 800. https://doi.org/10.1190/1.1484523.

Soula, J.C., 1982. Characteristics and mode of emplacement of gneiss domes and plutonic domes in central-eastern Pyrenees. J. Struct. Geol. 4 (3), 313-342. https://doi.org/10.1016/0191-8141(82)90017-7.

Soula, J.C., Debat, P., Brusset, S., Bessier, G., Christophoul, F., Deramond, J., 2001. Thrust-related, diapiric, and extensional doming in a frontal orogenic wedge: Example of the Montagne Noire, Southern French Hercynian Belt. J. Struct. Geol. 23 (11), 1677-1699. https://doi.org/10.1016/S0191-8141(01)00021-9.

Souza, Z.S., Kalsbeek, F., Deng, X.D., Frei, R., Kokfelt, T.F., Dantas, E.L., Li, J.W., Pimentel, M.M., Galindo, A.C., 2016. Generation of continental crust in the northern part of the Borborema Province, northeastern Brazil, from Archaean to Neoproterozoic. J. South Am. Earth Sci. 68, 68–96. https://doi.org/10.1016/j.jsames.2015.10.006.

Souza, Z.S., Oliveira, E.P., Cruz, L.B., Vilalva, F.C.J., 2019. Datação U-Pb em zirção de granito peraluminoso e granodiorito tipo Itaporanga, norte do lineamento Patos: implicações tectônicas. *In:* XXVIII Simpósio de Geologia do Nordeste, Aracajú.

Spector, A., Grant, F.S., 1970. Statistical models for interpreting aeromagnetic data. Geophysics. 35 (2), 293-302. https://doi.org/10.1190/1.1440092.

Talbot, C.J., 1974. Fold nappes as asymmetric mantled gneiss domes and ensialic orogeny. Tectonophysics. 24 (3), 259-276. https://doi.org/10.1016/0040-1951(74)90011-0.

Talwani, M., Worzel, J.L., Landisman, M., 1959. Rapid gravity computations for two-dimensional bodies with application to the Mendoncino submarine fracture zone. J. Geophys. Res. 64 (1), 49-59. https://doi.org/10.1029/JZ064i001p00049.

Teyssier, C., Whitney, D., 2002. Gneiss domes and orogeny. Geology. 30 (12), 1139-1142. https://doi.org/10.1130/0091-7613(2002)030%3C1139:GDAO%3E2.0.CO;2.

Tohver, E., D'Agrella-Filho, M.S., Trindade, R.I.F., 2006. Paleomagnetic record of Africa and South America for the 1200–500 Ma interval, and evaluation of Rodinia and Gondwana assemblies. Precambr. Res. 147, 199–222.

Tommasi, A., Vauchez, A., Daudré, B., 1995. Initiation and propagation of shear zones in a heterogeneous continental lithosphere. J. Geophys. Res. 100 (B11), 22083-22101. https://doi.org/10.1029/95JB02042.

Trompette, R., 1994. In: Geology of Western Gondwana (2000–500 Ma): Pan-African-Brasiliano Aggregation of South America and Africa. A.A Balkema, Rotterdam, Brookfield, pp. 350.

Trompette, R., 1997. Neoproterozoic (~600 Ma) aggregation of Western Gondwana: a tentative scenario. Precambrian Res. 82 (1-2), 101-112. https://doi.org/10.1016/S0301-9268(96)000459.

Van Schmus, W.R., Brito Neves, B.B., Hackspacher, P.C., Babinski, M., 1995. U/Pb and Sm/Nd geochronologic studies of the eastern Borborema Province, Northeast Brazil: initial conclusions. J. S. Am. Earth Sci. 8 (3-4), 267–288. https://doi.org/10.1016/0895-9811(95)00013-6.

Van Schmus, W.R., Brito Neves, B.B., Williams, I.S., Hackspacher, P.C., Fetter, A.H., Dantas, E.L., Babinski, M., 2003. The Seridó Group of NE Brazil, a late Neoproterozoic pre- to syn-collisional basin in West Gondwana: insights from SHRIMP U-Pb detrital zircon ages and Sm-

Nd crustal residence (TDM) ages. Precambrian Res. 127 (4), 281–327. https://doi.org/10.1016/S0301-9268(03)00197-9.

Vanderhaeghe, O., Teyssier, C., Wysoczanski, R., 1999. Structural and geochronological constraints on the role of partial melting during the formation of the Shuswap metamorphic core complex at the latitude of the Thor-Odin dome, British Columbia. Can. J. Earth Sci. 36 (6), 917-943. https://doi.org/10.1139/e99-023.

Vanderhaeghe, O., 2009. Migmatites, granites and orogeny: Flow modes of partially-molten rocks and magmas associated with melt/solid segregation in orogenic belts. Tectonophysics. 477 (3-4), 119-134. https://doi.org/10.1016/j.tecto.2009.06.021.

Vauchez, A., Neves, S.P., Caby, M., Corsini, M., Egydio Silva, M., Arthaud, M.H., Amaro, V., 1995. The Borborema shear zone system, NE Brazil. J. S. Am. Earth Sci. 8 (3-4), 247–266. https://doi.org/10.1016/0895-9811(95)00012-5.

Viegas, L.G.F., Archanjo, C.J., Hollanda, M.H.B.M., Vauchez, A., 2014. Microfabrics and zircon U–Pb (SHRIMP) chronology of mylonites from the Patos shear zone (Borborema Province, NE Brazil). Precambrian Res. 243, 1-17. https://doi.org/10.1016/j.precamres.2013.12.020.

Whitney, D.L., Teyssier, C., Vanderhaeghe, O., 2004. Gneiss domes and crustal flow. In: Whitney, D.L., Teyssier, C., Siddoway, C.S. (Eds.), Gneiss Domes in Orogeny. Geol. Soc. Am. Spec. Paper. vol. 380, pp. 15-33. https://doi.org/10.1130/0-8137-2380-9.15.

Yin, A., 2004. Gneiss domes and gneiss dome systems. In: Whitney, D.L., Teyssier, C., Siddoway, C.S. (Eds.), Gneiss Domes in Orogeny. Geol. Soc. Am. Spec. Paper. vol. 380, pp. 1-14. https://doi.org/10.1130/0-8137-2380-9.15.

Zhang, B., Chai, Z., Yin, C.Y., Huang, W.T., Wang, Y., Zhang, J.J., Wang, X.X., Cao, K., 2017. Intra-continental transpression and gneiss doming in an obliquely convergent regime in SE Asia. J. Struct. Geol. 97, 48-70. https://doi.org/10.1016/j.jsg.2017.02.010.

Zietz, I., Haworth, R.T., Williams, H., Daniels, D.L., 1980. Magnetic anomaly map of the Appalachian orogen. Memorial University of Newfoundland, Map No. 2a, scale 1:2,000,000.